

Hidden Heterogeneity: When to Choose Similarity-Based Calibration

Kiri L. Wagstaff

Thomas G. Dietterich

*School of Electrical Engineering and Computer Science
Oregon State University
Corvallis, OR 97331, USA*

KIRI.WAGSTAFF@OREGONSTATE.EDU

TGD@CS.ORST.EDU

Editor:

Abstract

Trustworthy classifiers are essential to the adoption of machine learning predictions in many real-world settings. The predicted probability of possible outcomes can inform high-stakes decision making, particularly when assessing the expected value of alternative decisions or the risk of bad outcomes. These decisions require well calibrated probabilities, not just the correct prediction of the most likely class. Black-box classifier calibration methods can *improve the reliability* of a classifier's output without requiring retraining. However, these methods are unable to detect subpopulations where calibration could *improve prediction accuracy*. Such subpopulations are said to exhibit "hidden heterogeneity" (HH), because the original classifier did not detect them. The paper proposes a quantitative measure for HH. It also introduces two similarity-weighted calibration methods that can address HH by adapting locally to each test item: SWC weights the calibration set by similarity to the test item, and SWC-HH explicitly incorporates hidden heterogeneity to filter the calibration set. Experiments show that the improvements in calibration achieved by similarity-based calibration methods correlate with the amount of HH present and, given sufficient calibration data, generally exceed calibration achieved by global methods. HH can therefore serve as a useful diagnostic tool for identifying when local calibration methods are needed.

Keywords: Classifier Calibration, Decision Making, Trustworthy Learning, Similarity-Based Methods, Hidden Heterogeneity

1. Introduction

How do we know when to trust a prediction? A predictive model is said to be *well calibrated* or *reliable* with respect to a distribution specified by $P(Y|X)$ if the probability it assigns to an outcome matches the true probability of that outcome according to $P(Y|X)$, for observation X and class label Y . Well-calibrated predictions are necessary for system trust and to minimize expected risk in cost-sensitive decision settings (e.g., medical diagnosis, autonomous driving, financial decisions). Likewise, calibration is necessary when combining or comparing predictions from different sources (Bella et al., 2013) or in classifier cascades that use a low-cost but less accurate classifier's output to decide whether to deploy a higher-cost but more accurate secondary classifier (Enomoto and Eda, 2021). Good calibration is beneficial in any decision making setting in which uncertainty matters (e.g., active learning or classification with a rejection or abstention option).

Concerns about poorly calibrated classifiers are not new (e.g., Zadrozny and Elkan, 2001; Niculescu-Mizil and Caruana, 2005). However, the recognition that deep neural networks in particular may sacrifice calibration to achieve higher generalization accuracy (Guo et al., 2017) has led to renewed interest in developing strategies to improve calibration. Several strategies have been invented including post-training calibration correction methods (e.g., Guo et al., 2017; Kumar et al., 2019; Kull et al., 2019; Alexandari et al., 2020), calibration-sensitive training methods (e.g., Kumar et al., 2018; Seo et al., 2019; Mukhoti et al., 2020), and adopting network architectures that do not use convolutions (Minderer et al., 2021). The latter two methods require access to the training data and resources to re-train a model, while post-training calibration does not. Consequently, post-training methods can be employed even when the training data (and model) are proprietary or when the data distribution has changed and we wish to recalibrate an existing classifier to extend its applicability. In general, these methods seek to devise a *calibration map* Φ that transforms the original predicted probabilities. Let the output of a classifier $f(x_i)$ applied to item x_i be a probability vector \hat{p}_i of length K (number of classes) that sums to 1 (i.e., resides in the simplex Δ_{K-1}). The calibration map $\Phi : \Delta_{K-1} \mapsto \Delta_{K-1}$ is derived from an independent calibration set C to transform \hat{p}_i to a more reliable $\hat{q}_i = \Phi(\hat{p}_i)$.

A key limitation of these calibration maps is the implicit assumption that all items with the same predicted posterior probability \hat{p} require the same correction. They cannot accommodate distinct subpopulations to which the classifier may have erroneously assigned the same \hat{p} value. For example, in predicting cancer risk, there could be many different reasons (age, lifestyle, family medical history, etc.) that a given individual has $\hat{p} = 0.9$. For some conditions, this probability could be an over-estimate, while for others, it could be an under-estimate. A global calibration map cannot accommodate this “hidden heterogeneity” (hidden by the classifier’s processing).

We propose a method to quantify hidden heterogeneity (HH) as a signal for when global calibration may be inadequate. We also develop two local calibration methods that customize calibration for each item x_i by leveraging its location in feature space to yield $\hat{q}_i = \Phi(\hat{p}_i|x_i)$. These methods determine the calibrated probability \hat{q}_i by taking a weighted vote of data points in the calibration set. The first method, Similarity-Weighted Calibration (SWC), assigns weights to every point in the calibration set based on similarity to x_i . This extends previous methods such as Similarity-Binning Averaging (Bella et al., 2009) that only consider the 10 most similar calibration points and do not weight them by similarity. The second method, SWC-HH, determines the size of the local neighborhood based on the estimated HH. We refer to the weighted number of calibration data points as the “similarity mass”. The similarity mass indicates how much calibration data was relevant for estimating \hat{q}_i . This measure of the quality of \hat{q}_i for each x_i is not provided by global calibration methods.

Figure 1 shows an example of the benefits of local calibration with SWC. In this setting, a linear support vector machine classifier was trained on 500 items to discriminate between two classes of handwritten MNIST digits, “4” and “9” (LeCun et al., 2010). For binary problems, we represent the classifier output $f(x_i) = \hat{p}_i$ as a scalar that is the probability $P(Y = 1|X = x_i)$. We denote the calibration map using lower-case $\phi : [0, 1] \mapsto [0, 1]$. Each panel in Figure 1 shows the 20 classification errors made by the SVM on an independent test set of 500 items. The x position of each digit corresponds to its $\hat{q}["9"]$, while its y

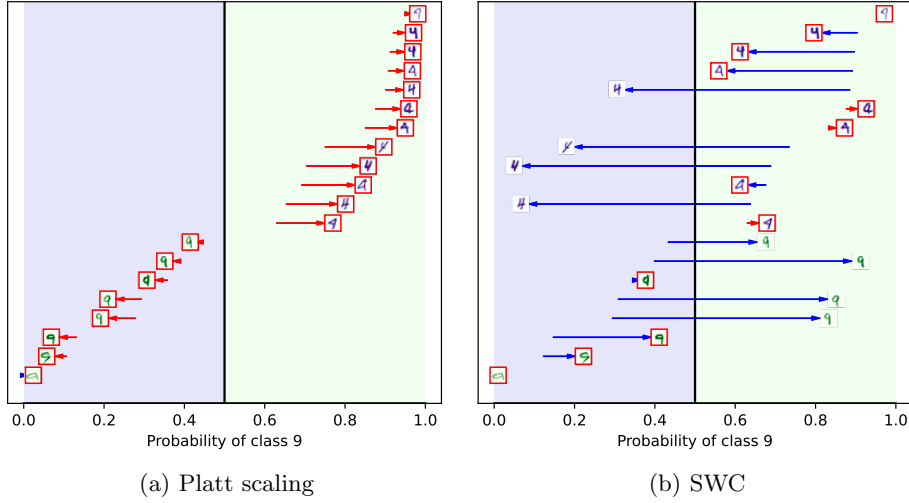


Figure 1: The effect of calibration on classifying handwritten digits “4” and “9” (errors framed in red). Arrows show changes from $\hat{p}["9"]$ to $\hat{q}["9"]$ (blue = beneficial, red = detrimental). Platt scaling pushes predictions more extremely incorrect, while SWC corrects 8 of the 20 errors and pushes all but three items closer to their true classes.

position is arbitrary (but consistent across panels) so that digits are visually separable. The arrows show the effect of calibration by pointing from $\hat{p}["9"]$ to $\hat{q}["9"]$, which is blue if $\hat{q}["9"]$ is more accurate and red if not. Platt scaling, a standard calibration mapping method (Platt, 1999) pushed these items to more extreme probabilities, emphasizing the wrong class (Figure 1(a)). In contrast, SWC corrected 8 of the 20 errors by reducing $\hat{q}["9"]$ for items in the “4” class and increasing it for items in the “9” class (Figure 1(b)). Only three items were nudged in the wrong direction, while Platt scaling pushed 19 items in the wrong direction (red arrows). The global Platt ϕ depends only on \hat{p} (x axis position), while the SWC ϕ is based on the similarity of each item to the calibration data.

The contributions of this paper are

- (a) Recommendations about how best to measure the quality of predicted probabilities (Section 2),
- (b) A method for quantifying hidden heterogeneity to indicate when local calibration is needed (Section 5), and
- (c) Two local calibration methods, Similarity-Weighted Calibration (SWC) (Section 4) and SWC-HH (Section 6).

We provide context from previous work in Section 3 and experimental results in Section 7. Key conclusions and limitations of similarity-based calibration are discussed in Section 8.

2. How do we measure the quality of probability predictions?

Most existing efforts to improve classifier reliability focus on the computation of “calibration error”, which is the absolute value of the difference between the predicted probabilities and

their true probabilities according to the target distribution. The expected value of this difference is known as the Expected Calibration Error (ECE) (Naeini et al., 2015).

2.1 Expected Calibration Error and its limitations

The challenge in measuring ECE is the need to estimate the true probabilities. This can be accomplished in two steps. First, we will assume that we have a labeled test data set sampled from the target distribution. This can be the same data set used to measure generalization ability via classification accuracy or other metrics. Let the test set consist of x_i and label y_i for $i \in \{1, \dots, N\}$, and let \hat{y}_i be the predicted class label with self-reported probability vector \hat{p}_i of size K , the number of classes. Second, we must choose some way of aggregating the test data to estimate the true probability. This is because each individual test point only gives us a single class label, and we need multiple samples from the conditional probability $P(\hat{y}|x_i)$ to estimate $P(\hat{y} = y|x_i)$, the probability according to $P(Y|X)$ that the true label is the one predicted by the classifier.

Many studies have performed the aggregation by discretizing the predictions \hat{p}_i into B bins and comparing the bin-weighted average “confidence” to the accuracy of predictions within the bin. Let the estimated accuracy of bin B_b containing N_b items be

$$Acc_b = \frac{1}{N_b} \sum_{\hat{p}_i \in B_b} \mathbb{1}(\hat{y}_i = y_i), \quad (1)$$

where $\mathbb{1}(c)$ is 1 if condition c is true and 0 otherwise. For binary problems, we compute the average predicted probability of class 1 in bin B_b as

$$Conf_b = \frac{1}{N_b} \sum_{\hat{p}_i \in B_b} \hat{p}_i, \quad (2)$$

while for multi-class problems we employ the maximum probability across all classes by indexing into the \hat{p}_i vector:

$$Conf_b = \frac{1}{N_b} \sum_{\hat{p}_i \in B_b} \operatorname{argmax}_k \hat{p}_i[k]. \quad (3)$$

Then for a test set with N items,

$$ECE = \sum_{b=1}^B \frac{N_b}{N} |Acc_b - Conf_b|. \quad (4)$$

Many researchers have pointed out limitations of this estimate, including sensitivity to the number and choice of bins (Vaicenavicius et al., 2019; Kumar et al., 2019; Patel et al., 2021) and undesirable edge effects (discontinuities at bin boundaries). Kumar et al. (2019) and Nixon et al. (2019) advocated employing equal-frequency bins instead of equally-spaced bins; the former proposed a “de-biased” squared calibration error to reduce sensitivity to the number of bins, and the latter proposed an Adaptive Calibration Error (ACE) metric that divides bins by population, computes error separately for each class, and then averages across classes. Even with these adjustments, any probability-binned ECE is problematic

due to the artificial partition of probability values into bins. Minderer et al. (2021) showed that equal-frequency bins with a different choice of number of bins can lead to contradictory conclusions about the relationship between calibration and accuracy. Different bin choices by different researchers have rendered published results incomparable. One way to reduce bin edge effects is to employ a kernel function to estimate calibration error without discrete bin boundaries, yielding smooth, local estimates of calibration error in probability space (Kumar et al., 2018; Zhang et al., 2020). However, kernel ECE methods require the specification of the kernel and its bandwidth and therefore still make comparisons difficult if different choices are made.

In addition to the issues of bin edge effects and lack of comparability between studies, calibration error metrics are insufficient for evaluation. They do not provide enough basis for preferring one method over another. Calibration error can be trivially minimized by always predicting the average probability of a given class across the whole data set, yielding perfectly calibrated but uninformative predictions (Kull et al., 2017; Widmann et al., 2019; Ovadia et al., 2019). Finally, ECE only compares accuracy to confidence for the predicted class, ignoring the calibration of predictions made for all remaining classes.

2.2 Brier Score

We therefore prefer to use the Brier score (Brier, 1950) for evaluating calibration methods, following many earlier researchers (e.g., Zadrozny and Elkan, 2001, 2002; Niculescu-Mizil and Caruana, 2005). The Brier score avoids the limitations of ECE and provides a holistic characterization of overall prediction quality. It computes the mean squared error between the predicted probability of *each* class and the true label, over a test set of N items. The Brier score sums over K classes, with $\hat{p}_i[k] \in [0, 1]$ indicating the predicted probability of class k for item i and y_i the true label of item i :

$$Brier(\hat{p}, Y) = \frac{1}{N} \sum_{k=1}^K \sum_{i=1}^N \left(\hat{p}_i[k] - \mathbb{1}(y_i = k) \right)^2. \quad (5)$$

This measure of error does not require a choice of binning or kernel. It combines reliability (calibration error), resolution (sharpness), and fundamental uncertainty (Bröcker, 2011; Ferro and Fricker, 2012). The “sharpness” component penalizes for lack of variance in the predicted probabilities, ensuring that the trivial solution mentioned above does not yield the best numeric result. In addition, the Brier score assesses the reliability of the predictions made for all classes, not just the highest scoring one, as has often been done with ECE on multiclass problems. Producing calibrated probabilities for all classes is important when computing expectations (e.g., for cost-sensitive classification). It is usually not needed when making rejection decisions.

3. Existing methods to improve classifier calibration

Classifiers can achieve better calibration using calibration-sensitive training methods, if the original training set is available (e.g., via modifications to the loss function proposed by Kumar et al., 2018; Mukhoti et al., 2020; Enomoto and Eda, 2021; Tomani and Buettner, 2021), using domain-specific representations that lead to improved calibration (Kalmady

et al., 2021), or using post-hoc calibration correction methods that modify the classifier’s predictions on new observations. We focus on the latter strategy since it requires no knowledge of the classifier’s details or access to the original training data.

Global, parametric calibration methods re-map the predicted probabilities output by the classifier, \hat{p} , by fitting a desired functional form (e.g., logistic curve) from the probabilities to the labels to compute $\hat{q} = \Phi(\hat{p})$. For binary classifiers, Platt scaling (Platt, 1999) transforms \hat{p}_i into a value between 0 and 1 using a sigmoid function with two parameters, A and B : $\hat{q}_i = \frac{1}{1+e^{A\hat{p}_i+B}}$. The parameters A and B are chosen to optimize the negative log-likelihood of predictions made on the calibration set. Platt scaling was generalized to multi-class problems for neural networks (Guo et al., 2017) via a method called temperature scaling, which operates on the logits z_i (not the probabilities) by optimizing temperature parameter T in $u_i[k] = e^{z_i[k]/T}$, where $z_i[k]$ is the logit for item i and class k , and $u_i[k]$ is the corresponding unnormalized probability. These values are normalized as $\hat{q}_i[k] = \frac{u_i[k]}{\sum_j u_j[k]}$. The same T value is used for all classes. Bias-Corrected Temperature Scaling (Alexandari et al., 2020) adds a bias term for each class.

There are also several approaches that construct bins and calibrate the items within each bin by assigning the average (or other aggregate) accuracy within that bin B_b as the calibrated probability, $\hat{q}_i = Acc_b, \forall i \in B_b$. Histogram binning (Zadrozny and Elkan, 2001) assigns items to bins based on their uncalibrated predictions \hat{p}_i , often using equally-spaced bin boundaries or divided so that each bin has the same number of items (“equal frequency”) from the calibration set. Kumar et al. (2019) show that the latter strategy, as well as using a larger number of bins, yields better results. Isotonic regression (Zadrozny and Elkan, 2002) adds further flexibility by optimizing the bin boundaries to minimize the squared loss between \hat{q}_i and y_i . Recently, Patel et al. (2021) proposed selecting the bin boundaries to maximize the mutual information between bin predictions \hat{q}_i and y_i .

To date, very few calibration methods have leveraged the location of items in feature space, \mathcal{X} . Instead, most methods encode the strong assumption that all items with the same uncalibrated probability \hat{p} should map to the same calibrated value \hat{q} . The LoRe calibration method relaxes this assumption somewhat by computing a “confidence” that is weighted by item similarity but is still confined to a pre-specified probability bin (Luo et al., unpublished). Our approach uses the whole calibration set rather than only items within a pre-specified probability bin, and it estimates the full posterior distribution across classes $\hat{q}_i[k], \forall k$. The LoRe output confidence applies only to the highest probability class according to \hat{p}_i , and since probability mass is not redistributed across classes, the class distribution is lost.

A calibration approach that uses similarity to compute the complete $\hat{q}_i[k]$ vector is Similarity-Binning Averaging or SBA (Bella et al., 2009), which creates bins (neighborhoods) based on an item’s 10 nearest neighbors in an “augmented” feature space $\mathcal{X}^+ = \mathcal{X} \times \Delta_{K-1}$ defined by the item’s feature vector x_i of dimension d concatenated with its probability vector $\hat{p}_i \in \Delta_{K-1}$. SBA computes the calibrated probability $\hat{q}_i[k]$ as the probability of class k (in the calibration set) within item i ’s assigned bin, with each item contributing equally (no weighting). In contrast, our approach uses a similarity-weighted contribution from each item in the calibration set, not just the 10 nearest neighbors. Zhao et al. (2020) introduced “individual” calibration, which emphasizes good calibration for each item rather than in aggregate over the whole data set. While this approach is specific to regression and

Algorithm 1 Similarity-Weighted Calibration (SWC)**Input:** Test item t , calibration data $x_i \in C$ and labels y_i **Output:** Calibrated probabilities $\hat{q}_t[k], \forall k$

- 1: Collect model predictions for item t : $\hat{p}_t[k]$ for $k \in \{1 \dots K\}$.
- 2: Collect model predictions for the calibration set: $\hat{p}_i[k]$ for $x_i \in C, k \in \{1, \dots, K\}$.
- 3: Compute pairwise similarity as $s(t, i)$ for $x_i \in C$.
- 4: Compute $\hat{q}_t[k] = \frac{1}{\sum_i s(t, i)} \sum_i s(t, i) \mathbb{1}(y_i = k)$ for $k \in \{1, \dots, K\}$ (Eqn. 6).

the construction of well-calibrated confidence intervals, its motivation is similar to that which inspired the creation of SWC for classification problems.

4. Similarity-Weighted Calibration (SWC)

We propose to calibrate classifier predictions by leveraging information in feature space as well as the uncalibrated probabilities \hat{p}_i . Given test item t , the goal is to estimate well-calibrated $\hat{q}_t[k] = P(y = k|x_t)$ for each class $k \in \{1 \dots K\}$. This approach to calibration, Similarity-Weighted Calibration (SWC), is described in Algorithm 1. Let

$$s(t, i) = \text{sim}(\langle x_t, \hat{p}_t \rangle, \langle x_i, \hat{p}_i \rangle) \in [0, 1]$$

be the similarity between item t and item i measured in the augmented space \mathcal{X}^+ . A similarity of 1 is perfect identity. (We will discuss the choice of similarity function sim below.) SWC computes the similarity of t to every item in the calibration set (step 3) and uses this information to replace \hat{p} with a similarity-weighted combination of labels from the calibration set (step 4).

$$\hat{q}_t[k] = \frac{1}{\sum_i s(t, i)} \sum_i s(t, i) \mathbb{1}(y_i = k) \quad (6)$$

The similarity-based approach to calibration enables specialization for different populations within the data set. Global methods assume that all items with the same predicted probability require the same correction, while local methods allow the possibility that one prediction is over-confident while another is under-confident, even if they have the same predicted probability.

As noted above, SWC differs from SBA in that it uses a weighted sum across all items in the calibration set rather than averaging the labels of the 10 nearest neighbors. Like SBA, similarity is computed in augmented feature space. The choice of similarity measure is a key ingredient in any similarity-based calibration method. SBA uses the Weka IBk implementation of the k-nearest-neighbors algorithm, applied to the augmented feature space defined by concatenating the data feature vector with the probability vector. By default, IBk employs Euclidean distance.

We have found a supervised similarity function known as the random forest *proximity function* (RFprox) to be very effective. RFprox trains a random forest on a labeled data set and defines the similarity between items x_i and x_j as the fraction of times they are assigned to the same leaf in each tree of the ensemble (Breiman, 2001; Cutler et al., 2012).

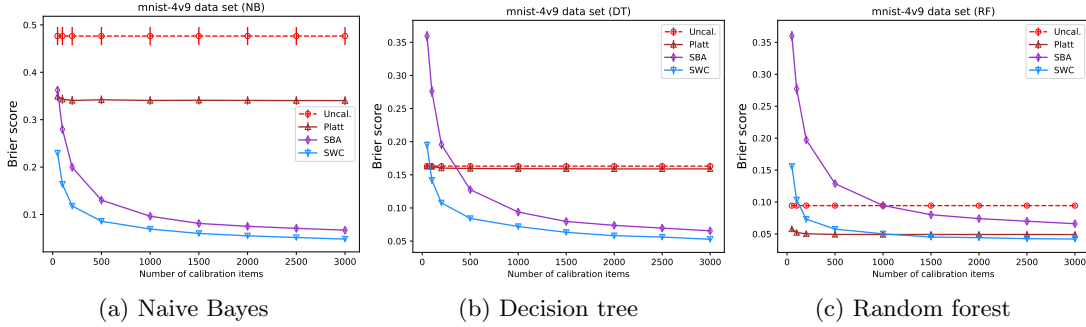


Figure 2: Learning curves showing Brier score (lower is better) as a function of the calibration set size for the MNIST 4-vs-9 data set, using different calibration methods with three classifiers. Error bars show one standard error over 10 trials.

Hastie et al. (2009) noted that a random forest is effectively a weighted version of the k-nearest-neighbors classifier with an “equivalent kernel” defined by those weights (leaf co-occurrences), and Scornet (2016) described how the random forest can be rewritten as a kernel function itself. We employ the calibration data to learn the relevant RFprox measure.

Figure 2 displays learning curves that illustrate the differences between calibration methods on a binary classification problem in which the goal is to distinguish two handwritten digits (“4” vs. “9”) from the MNIST data set (LeCun et al., 2010). In this experiment, a classifier of the indicated type was trained on 500 randomly chosen items and tested on another set of 500 randomly chosen items. A third randomly chosen selection of data constituted the calibration set, and the size was varied from 100 to 2000 items. Results were averaged over 10 randomly seeded trials. The uncalibrated predictions for the classifiers yielded different starting Brier scores. Platt scaling improved the Brier score for the Naive Bayes (NB) and random forest (RF) classifiers but only marginally for the decision tree (DT). No further improvements were achieved beyond 500 calibration items. Similarity-based calibration (SBA and SWC) achieved much larger benefits for NB and DT when at least 500 items were used for calibration, and Brier score continued to improve as more calibration data was provided. The random forest, which had the best initial Brier score and therefore less room for improvement, showed an advantage for similarity-based calibration after at least 1500 items were used.

The SWC approach, using the RFprox similarity measure, out-performed SBA, which uses Euclidean distance. RFprox is not constrained to treat distance in each dimension equally. Since RFprox uses labels to learn the similarity measure, it can elevate the importance of individual features in X^+ (like $\hat{p}[k]$) by placing them higher in individual decision trees within its ensemble. In addition, SWC weights evidence from the entire calibration set rather than the 10 nearest neighbors as SBA does. A final difference between SBA and SWC is that SBA showed almost no difference in Brier score for different classifiers (note difference in y axis scale for panels in Figure 2). This data set is represented by 784 features, so the addition of two dimensions in augmented feature space (by concatenating \hat{p}) had little effect. In contrast, SWC yielded different absolute results for each classifier

because RFprox can effectively achieve feature weighting and was more influenced by the different \hat{p} values provided by each classifier.

5. Hidden heterogeneity

In the published literature—and in our own experiments—we find that global post-hoc calibration methods, such as Platt scaling and temperature scaling, perform very well for some data sets and algorithms and less well for others. Similarly, local methods do not always improve upon these global methods. What causes the failure of global methods, and under what conditions can local methods do better? Our hypothesis is that global post-hoc calibration fails when the data exhibits *hidden heterogeneity* (HH) with respect to the predicted probabilities \hat{p} . HH occurs when there are subpopulations in the feature space \mathcal{X} to which the classifier assigns the same \hat{p} but that require different calibration corrections.

Definition 1 *A classifier f exhibits hidden heterogeneity with respect to a feature space \mathcal{X} if there exists a subregion $\mathcal{U} \subseteq \mathcal{X}$ such that $f(x) \approx \hat{p}$ for all $x \in \mathcal{U}$ and yet \mathcal{U} can be partitioned into M disjoint subregions $\mathcal{U} = \mathcal{U}_1 \cup \dots \cup \mathcal{U}_M$ such that the true class probabilities $P(y|x \in \mathcal{U}_m) \neq P(y|x \in \mathcal{U}_{m'})$ for all distinct pairs $m, m' \in \{1, \dots, M\}, m \neq m'$.*

An extreme example of HH occurs for a classifier that ignores all features and predicts the majority class for all items. Imagine a data set composed of 60% cats and 40% birds. A classifier that predicts $P(y = \text{"cat"}) = \hat{p} = 0.6$ for all items (i.e., $\mathcal{U} = \mathcal{X}$) would have a “perfect” ECE of 0 but a non-zero Brier score, since the latter is sensitive to “sharpness” as well as calibration. In this setting, global calibration methods cannot improve the result, because any $\Phi(\hat{p})$ must map all items to the same new \hat{q} , for which any value other than 0.6 would increase the Brier score (or ECE). Now suppose that the items have a feature such as “number of legs”. Then two subregions— \mathcal{U}_1 for animals with two legs and \mathcal{U}_2 for animals with four legs—can be defined with true conditional probabilities of 1 (for “cats”) and 0 (for “birds”). In such cases, individual calibration could model these subregions separately and assign \hat{q}_i differently for \mathcal{U}_1 and \mathcal{U}_2 .

The extent to which hidden heterogeneity can be detected is determined by the representation of the input space \mathcal{X} . Consider a domain in which items from multiple classes are not separable given their feature space representation. In this case, the uncertainty in the class label is aleatory and irreducible. However, if the input representation makes it possible to separate the classes (e.g., based on number of legs), then the uncertainty is epistemic (model-specific) and could be detected by a different model.

There are many reasons why a learned model might exhibit hidden heterogeneity. First, the training data set might not have been large or diverse enough to reveal the heterogeneity. Second, global regularization may have forced the learned function f to be too smooth in some regions of the input space. A third case arises when the test distribution is different than the training distribution. The learned function could have no hidden heterogeneity with respect to the training distribution and yet show hidden heterogeneity on the test set.

Given a calibration data set C sampled from the same distribution as the test set, we can approximate the *detectable* hidden heterogeneity for a region $\mathcal{U} \subseteq C$ as the potential improvement (compared to the original classifier) achieved by training a specialized classifier on only the items in \mathcal{U} . We define \mathcal{U} in terms of a neighborhood of points with very similar

predicted probabilities \hat{p} . Specifically, we compare the Brier score (with respect to true labels $Y = \{y_i\}$) of the original predictions by model f on \mathcal{U} with those generated by a new model g :

$$HH_{\mathcal{U},Y} = Brier(f(\mathcal{U}), Y) - Brier(g(\mathcal{U}), Y). \quad (7)$$

For a given test item t , a new (local) classifier g is trained using only the nearby calibration items in \mathcal{U}_t , and it generates predictions for use in Equation 7 to compute $HH_{\mathcal{U}_t,Y}$. We enforce the condition that g is no worse than f by clipping $HH_{\mathcal{U},Y}$ to 0.

We define item t 's probability neighborhood \mathcal{U}_t to contain calibration items that are close to t in the probability simplex Δ_{K-1} . More precisely, \mathcal{U}_t contains the items within radius r of item t in Δ_{K-1} . We employ Hellinger distance to calculate the distance between two probability vectors \hat{p}_i and \hat{p}_j :

$$H(\hat{p}_i, \hat{p}_j) = \frac{1}{\sqrt{2}} \sqrt{\sum_{k=1}^K \left(\sqrt{\hat{p}_i[k]} - \sqrt{\hat{p}_j[k]} \right)^2}. \quad (8)$$

Conveniently, this can be expressed as the Euclidean norm of the difference of the element-wise square root of each probability vector (Krstovski et al., 2013):

$$H(\hat{p}_i, \hat{p}_j) = \frac{1}{\sqrt{2}} \left\| \sqrt{\hat{p}_i} - \sqrt{\hat{p}_j} \right\|_2. \quad (9)$$

This in turn allows the use of efficient methods (e.g., k-d tree) for populating \mathcal{U}_t .

The specialized classifier g that is trained to output local probabilities for \mathcal{U}_t can be any classifier type. We employed an ensemble method that can perform internal generalization estimates without an additional validation set. We trained a bagged ensemble of 50 decision trees with no depth limit and no limit on the number of features searched for each split. We used out-of-bag error to determine how much pruning to employ to achieve good generalization and avoid overfitting to the calibration set. We searched over 7 values of the α pruning complexity parameter, evenly spaced between 0.0 (no pruning) and 0.03, as input to the minimal cost-complexity pruning method (Breiman et al., 1984).

Figure 3 shows the improvement (reduction) in Brier score after calibration as a function of the average HH across the test set. In each experiment, we randomly selected 500 training items, 500 test items, and 1000 calibration items for four binary MNIST problems: “1” vs. “7” (relatively easy), “4” vs. “9” and “3” vs. “8” (intermediate), and “3” vs. “5” (difficult). HH was calculated using a probability radius of 0.1. We trained a variety of classifiers and used Platt scaling and SWC to calibrate their predictions on the test set, using 10 trials per combination of data set and classifier. Platt scaling was most effective for problems with low HH. In contrast, SWC yielded Brier score improvements that correlate strongly with the amount of HH present ($\rho = 0.99$).

This experiment shows that HH, which can be computed prior to calibration, is a useful diagnostic indicator that can guide the choice of calibration strategy as well as the key factor that explains when and why local calibration yields improvements. When HH is high, it is advisable to employ a similarity-based calibration method like SWC. When HH is low, global methods such as Platt scaling may be sufficient.

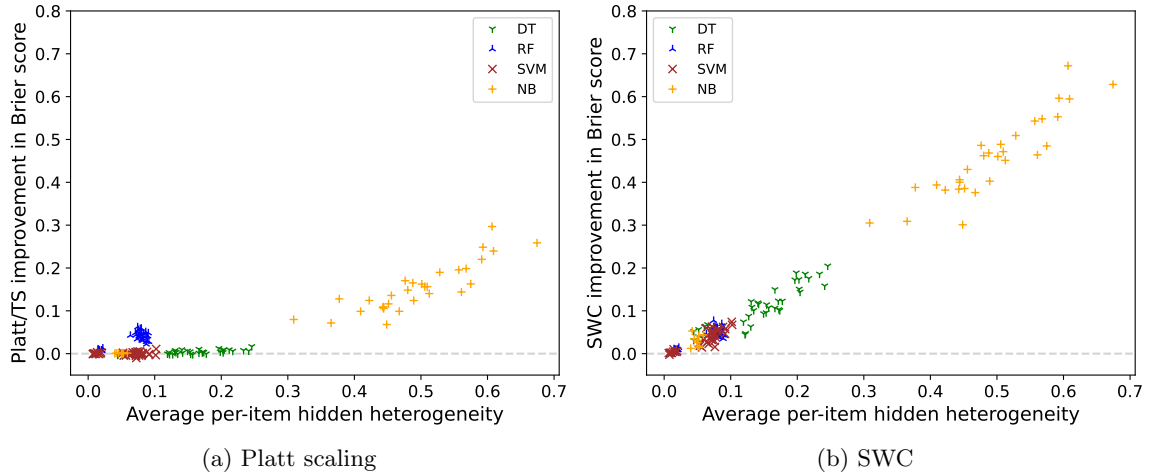


Figure 3: Brier score improvement as a function of average hidden heterogeneity for Platt scaling and Similarity-Weighted Calibration (SWC) with 3000 calibration items and 10 random trials for each classifier type across four **binary** MNIST problems.

We investigate the benefits of similarity-based calibration with more extensive experiments in Section 7. First, however, we propose a second approach, SWC-HH, that explicitly incorporates HH into the calibration process.

6. Similarity-Weighted Calibration with Hidden Heterogeneity (SWC-HH)

Given that SWC achieves Brier score improvements that correlate with HH, a natural next question is whether explicitly incorporating HH into the calibration process could yield further improvements. We developed a variant of SWC that filters the calibration set to restrict which items are used to generate \hat{q} (see Algorithm 2; changes from SWC are indicated in red). HH, which is computed separately for each test item t , is provided as an additional input for calibration. Step 4 uses this value to restrict which items x_i from the calibration set contribute to \hat{q} . SWC-HH only includes items with a similarity to item t of at least $\frac{1}{2}HH_{t,y}$. Note that the maximum value for HH is 2.0 since it is the difference in Brier scores, clipped to 0.0, and each Brier score ranges between 0.0 and 2.0. Dividing by 2.0 normalizes the threshold to the range 0.0–1.0, making it suitable as a similarity threshold.

Figure 4 shows results for the same experiments reported in Figure 2, with the addition of SWC-HH. We found that SWC-HH yielded a clear advantage at all calibration set sizes for NB and DT, and it also provided a small advantage over SWC for RF with calibration set sizes larger than 1500 items. These initial results support our hypothesis that explicit incorporation of HH can yield better similarity-based calibration outcomes.

Algorithm 2 Similarity-Weighted Calibration with Hidden Heterogeneity (SWC-HH)**Input:** Test item t , calibration data $x_i \in C$ and labels y_i , **hidden heterogeneity** $HH_{\mathcal{U}_t, \mathcal{Y}}$ **Output:** Calibrated probabilities $\hat{q}_t[k], \forall k$

- 1: Collect model predictions for item t : $\hat{p}_t[k]$ for $k \in \{1 \dots K\}$.
- 2: Collect model predictions for the calibration set: $\hat{p}_i[k]$ for $x_i \in C, k \in \{1, \dots, K\}$.
- 3: Compute pairwise similarity as $s(t, i)$ for $x_i \in C$.
- 4: Compute $\hat{q}_t[k] = \frac{1}{\sum_i s(t, i)} \sum_i s(t, i) \mathbb{1}(y_i = k)$ **s.t.** $s(t, i) \geq \frac{1}{2} HH_{\mathcal{U}_t, \mathcal{Y}}$ for $k \in \{1, \dots, K\}$.

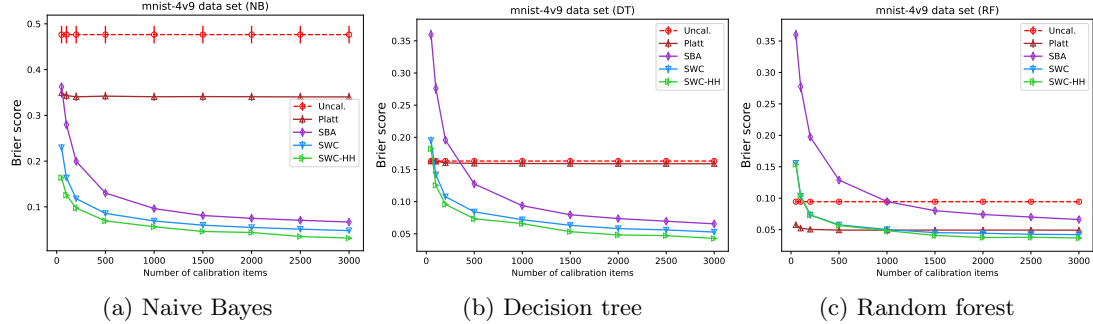


Figure 4: Learning curves showing Brier score (lower is better) as a function of the calibration set size for the MNIST 4-vs-9 data set, using different calibration methods (including SWC-HH) with three classifiers. Error bars show one standard error over 10 trials.

7. Experimental results

We conducted experiments with a variety of classifiers and data sets to compare local and global calibration methods and to determine the role that hidden heterogeneity plays. Our hypotheses were that (1) local, similarity-based calibration would be more effective at reducing Brier score than global calibration methods, (2) the amount of improvement would correlate with the hidden heterogeneity score, and (3) similarity mass could serve as an indicator of calibration set relevance. Our implementations of SWC, SWC-HH, and other calibration methods, along with scripts to replicate the experiments, are available at <https://github.com/wkiri/simcalib>.

7.1 Methodology

We assessed calibration methods over a suite of different classifiers as implemented in the scikit-learn Python library (Pedregosa et al., 2011). For tabular data, we employed a decision tree with `min_samples_leaf = 10` (DT), a random forest with 200 trees (RF), an ensemble of 200 gradient-boosted trees (GBT), a linear support vector machine (SVM), a Gaussian kernel ($\gamma = \frac{1}{d \text{var}(X)}$, $C = 1.0$) vector machine (RBFSVM), and a Naive Bayes classifier (NB). Any parameters not explicitly mentioned were set to their default values. We also conducted experiments with pre-trained deep neural networks from large image data sets.

For tabular data sets, we randomly sampled 10,000 items and randomly split them into 500 train, 500 test, and 9000 for a calibration pool. For the “mnist10” and “letter” data sets, we used 1000 items each for training and test, due to their large number of classes (10 and 26, respectively). We calibrated each trained model using a series of nested calibration sets of size $\{50, 100, 200, 500, 1000, 1500, 2000, 2500, 3000\}$ to assess the data efficiency of each calibration method. When using a pre-trained classifier, we generated a class-stratified random split of the standard test set into 5000 test items and used the remainder as the calibration set. We report average performance across 10 trials along with the standard error for the observed values.

Calibration methods. We compared three similarity-based calibration methods (SBA, SWC, and SWC-HH) to standard calibration methods including Platt scaling (Platt, 1999) and histogram binning (Zadrozny and Elkan, 2001). SBA calibrates each item using its 10 nearest neighbors in an augmented feature space that concatenates the original feature space with the K uncalibrated class probabilities $\hat{p}[k]$ (Bella et al., 2009). Our implementation of SBA employs Euclidean distance to identify the nearest neighbors, which we believe to be the method used by Bella et al. SWC and SWC-HH used the RFprox similarity measure. When computing hidden heterogeneity, we used a probability radius of $r = 0.1$ in the probability simplex.

Our implementation of Platt scaling optimizes the negative log-likelihood of predictions against the target probabilities rather than discrete $\{0, 1\}$ labels (Platt, 1999; Niculescu-Mizil and Caruana, 2005). With n_+ as the number of calibration items in the positive class and n_- as the number of negative items, the target probabilities are

$$y_+ = \frac{n_+ + 1}{n_+ + 2}; \quad y_- = \frac{1}{n_- + 2}.$$

For multi-class problems, we applied temperature scaling (Guo et al., 2017) in the place of Platt scaling, which is limited to binary decisions. For classifiers that output probabilities instead of logits, we first transformed \hat{p}_i into logits as $z_i[k] = \ln \frac{\hat{p}_i[k]}{1 - \hat{p}_i[k]}$. To avoid dividing by or taking the logarithm of zero, we clipped $\hat{p}_i[k]$ to the range $[\epsilon, 1 - \epsilon]$, where $\epsilon = 1 \times 10^{-12}$. We used the histogram binning method implemented by Kumar et al. (2019)¹ and followed their recommendation to use equal-mass bins (100 bins).

Data sets. We conducted experiments with several commonly used tabular and image data sets. The tabular data sets include:

- moons: a synthetic 2D data set composed of two partially overlapping classes, chosen to enable visualization of classifier outputs and hidden heterogeneity in feature space. We randomly generated observations using the scikit-learn `make_moons()` function with `noise` set to 0.3 and `random_state` set to 0.
- letter (letter recognition): a 26-class data set of capital letters from the English alphabet represented by 16 statistical and geometrical features that describe the image of the letter. The data is available from the UCI repository at <https://archive.ics.uci.edu/ml/datasets/letter+recognition>.

1. Available at https://github.com/p-lambda/verified_calibration.

- mnist: the MNIST handwritten digit data set (LeCun et al., 2010) composed of 28x28 pixel ($d = 784$) images containing a digit from 0 to 9. We used the data set as provided by OpenML, with the original source of <http://yann.lecun.com/exdb/mnist/>. In addition to the 10-class data set (mnist10), we created several binary subsets consisting only of two digits, such as “4” and “9” (mnist-4v9). We treat this data set as “tabular” in that each image is represented as a one-dimensional feature vector (no 2D image structure is preserved).
- fashion-mnist: this data set consists of grayscale images of articles of clothing and accessories (10 classes) that was designed to be more challenging than the MNIST data set yet have the same dimensionality (28x28, $d = 784$) (Xiao et al., unpublished). The data is available at <https://github.com/zalandoresearch/fashion-mnist>.

The image data sets include:

- CIFAR-10: 60,000 images (64×64 pixels) labeled into 10 distinct classes; the test set contains 10,000 images (Krizhevsky, 2009)
- CIFAR-100: a disjoint set of 60,000 images labeled into 100 different classes (50k train, 10k test)

Metrics. As discussed in Section 2, we employ Brier score as an overall measure of prediction quality. We also report classification accuracy. We do not independently report an ECE value due to the issues associated with this measure that were identified in Section 2. The combination of Brier score and classification accuracy better characterizes prediction quality across all classes and without artificial discretization and edge effects. To likewise avoid the drawbacks of binning-based depictions for reliability diagrams, including coarse granularity and discontinuities at bin boundaries, we use the kernel density estimation approach developed by Zhang et al. (2020), which estimates the accuracy for each test item using a triweight kernel in probability space.

7.2 Results

7.2.1 HIDDEN HETEROGENEITY AND CALIBRATION

We visualize the calibration process in Figure 5 for the two-dimensional “moons” data set. Each row corresponds to results for a different classifier (linear SVM, decision tree, and random forest). The third column shows the computed hidden heterogeneity (HH) values. The linear SVM cannot model the nonlinear decision boundary very well. This region, where the classes are mixed yet separable in the feature space, has a high value for HH. This band corresponds to \hat{p} values that are adapted most strongly by SWC, yielding a decrease (improvement) in Brier score from 0.218 to 0.133. Platt scaling increases (worsens) the Brier score slightly. The decision tree (second row of Figure 5) exhibits less hidden heterogeneity on the same data set, because it is able to model the nonlinear decision boundary more effectively. SWC improves the predictions and Brier score from 0.156 to 0.129. Finally, the random forest (bottom row of Figure 5) with its more complex decision boundary has more areas with hidden heterogeneity. SWC generally results in smoother regions as the calibration data informs updates to the posterior probabilities, improving Brier score from 0.134 to 0.122.

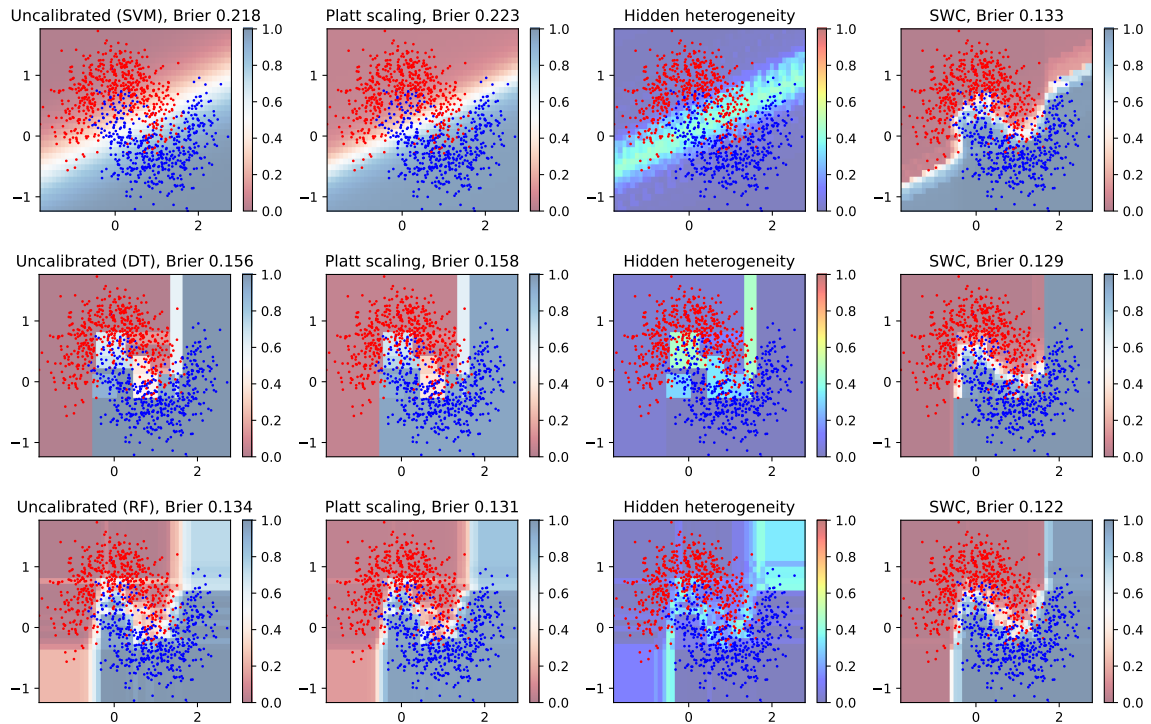


Figure 5: Visualization of uncalibrated predictions (first column) for the “moons” data set, Platt scaling (second column), and SWC (fourth column). The third column shows hidden heterogeneity values that highlight areas of potential improvement, which align with SWC improvements.

Importantly, the difference in results for the rightmost column in Figure 5 demonstrates that SWC adapts (calibrates) most where the classifier exhibits hidden heterogeneity, yielding a result that is customized to the original classifier and more flexible than global calibration.

7.2.2 CALIBRATION OF TABULAR DATA CLASSIFIERS

We found that similarity-based calibration is effective for both binary and multi-class data sets. Figure 6 presents results across all classifiers and calibration methods for the “mnist-4v9”, “mnist10”, and “fashion-mnist” data sets, after 3000 (binary) or 5000 (multi-class) calibration items were employed. Numerical values for these results are provided in Appendix A, Tables 2, 8, and 9. Classifiers appear in order of improving (decreasing) Brier score for the uncalibrated predictions. Platt scaling improved performance primarily for the Naive Bayes and random forest classifiers, but it yielded little benefit for the others. Temperature scaling improved performance for the tree-based methods (RF, GBT) the most, although not consistently. Histogram binning performed about the same as Platt/TS, except for Naive Bayes models where it was much better. However, similarity-based methods were highly effective for all classifiers in reducing Brier score. The improvement correlates with the average HH value, shown in parenthesis under the x axis labels.

In addition, similarity-based calibration also increased test accuracy (see right column of Figure 6). SWC-HH consistently achieved the highest accuracy. However, for the more challenging “fashion-mnist” data set, SWC achieved the best Brier score, which more accurately reflects calibration. In this data set, the filtering employed by SWC-HH (to ignore calibration items with similarity less than HH) often leaves no calibration items remaining. We handle this case by using the single nearest neighbor, even if its similarity is below the threshold. This leads to values for \hat{q} that are based only on one calibration item. In many cases, the single nearest neighbor belongs to the correct class, yielding good accuracy, but when it is from an incorrect class, the Brier score penalty is large.

Results for additional MNIST binary data sets are available in Appendix A: “mnist-1v7” (easy) in Table 3, “mnist-3v8” (intermediate) in Table 4, and “mnist-3v5” (hardest) in Table 5. They exhibit the same behavior as shown for “mnist-4v9” in Figure 6, with the best results obtained using SWC-HH. For the “moons” data set, using 3000 calibration items yields ties between SBA and SWC for Brier score, and ties for SBA, SWC, and SWC-HH (Table 6). All similarity-based methods out-performed the global methods.

We also found that temperature scaling (with multi-class problems) is even less robust to the presence of hidden heterogeneity than Platt scaling (with binary problems). Figure 7 shows the improvements in Brier score as a function of HH for multi-class problems (“mnist10”, “fashion-mnist”, and “letter”). The improvements obtained by Platt scaling for high-HH problems and the Naive Bayes classifier do not carry over to these multi-class problems. However, SWC exhibits strong improvements in Brier score that correlate well with HH, as shown in Figure 7(b). The correlation of improvement with HH is -0.38 for temperature scaling but 0.91 for SWC.

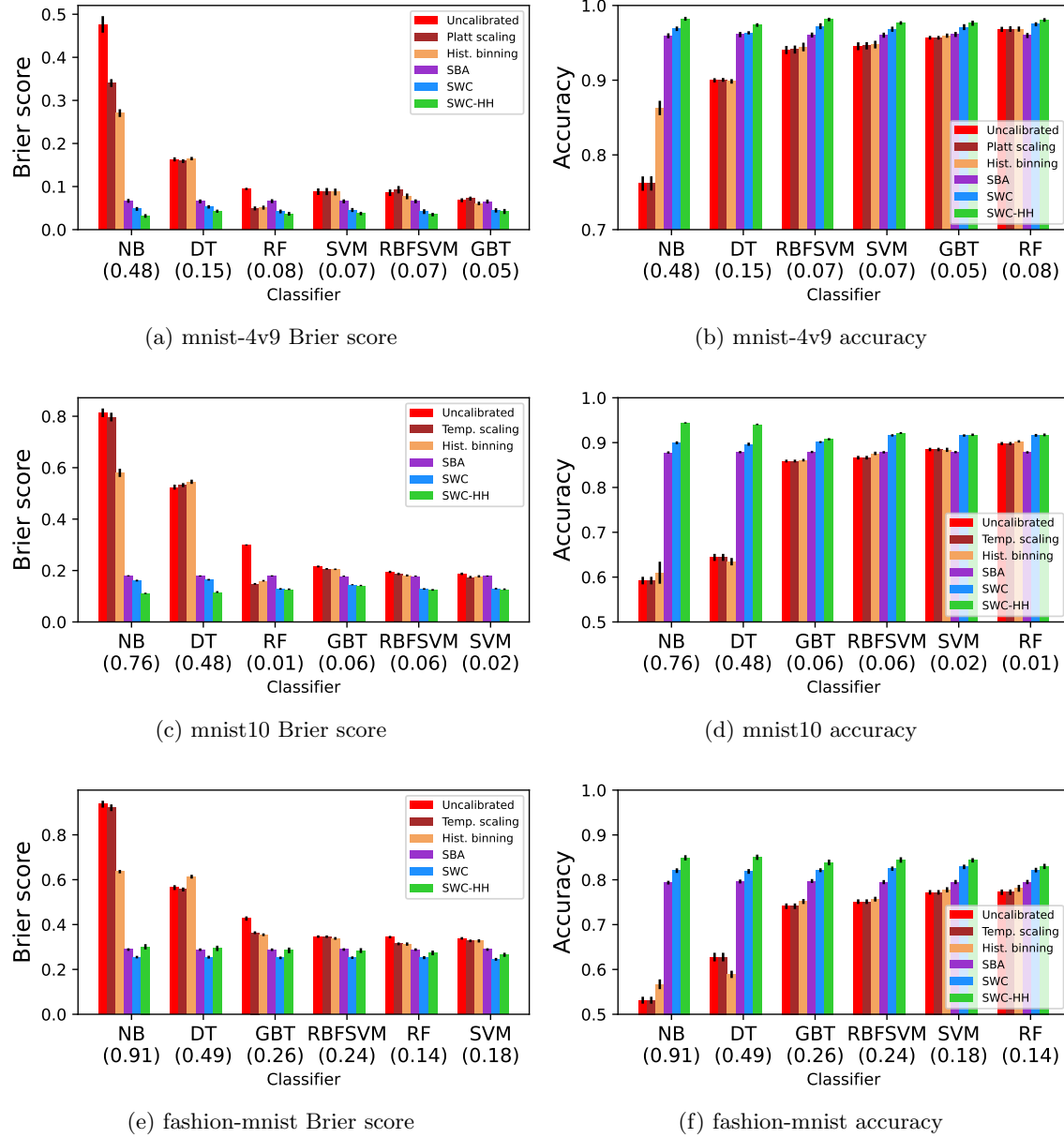


Figure 6: Calibration performance (left) and accuracy (right) for the binary “mnist-4v9” and multi-class “mnist10” and “fashion-mnist” data sets (10 trials; error bars indicate one standard error). Classifiers are sorted in order of improvement based on the uncalibrated classifier’s score, and average HH values are below each classifier.

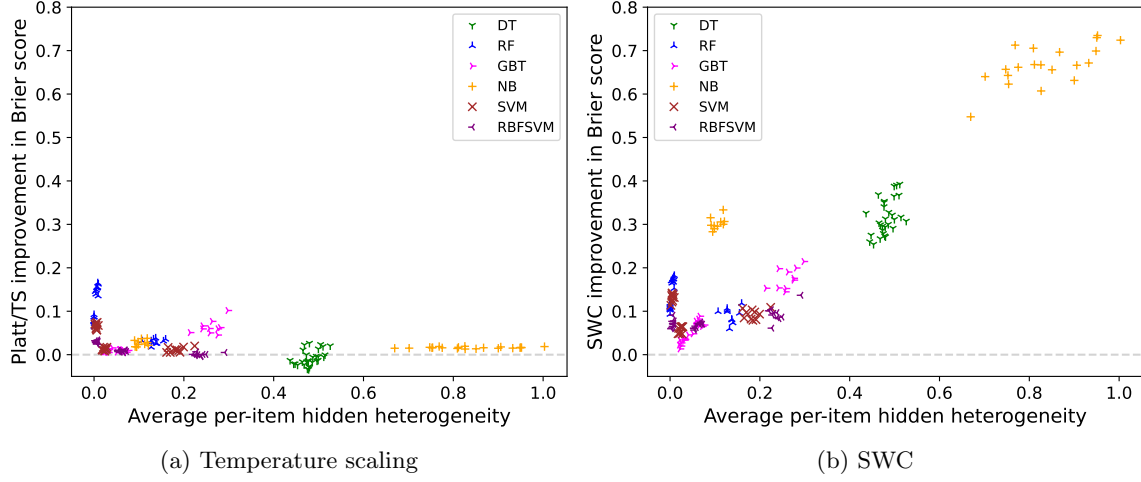


Figure 7: Brier score improvement as a function of average hidden heterogeneity for temperature scaling and Similarity-Weighted Calibration (SWC) with 5000 calibration items and 10 random trials for each classifier type across three **multi-class** problems.

7.2.3 CALIBRATION OF IMAGE CLASSIFIERS

We also conducted calibration experiments with the CIFAR-10 and CIFAR-100 data sets (Krizhevsky, 2009) using three pre-trained neural networks of increasing complexity². ResNet20 (He et al., 2016) has 20 layers and 0.27M parameters, ResNet56 (He et al., 2016) has 56 layers and 0.85M parameters, and RepVGG_A2 (Ding et al., 2021) has 22 layers and 25.49M parameters. For these data sets, the similarity measure *sim* operates in the latent space learned by each network. Specifically, we used the output activations of the `avgpool` (for ResNet models) and `gap` (for RepVGG_A2) layers as a feature vector (dimensionality 64, 64, and 1408 respectively) for similarity computations. We again used a learned RF proximity function to compute similarity. We conducted 10 trials that each perform a class-stratified random split of the standard 10,000-item test set into 5000 items for calibration and 5000 items for testing. We found that a probability radius of 0.05 yielded reasonably sized neighborhoods for computing HH.

The results of applying similarity-based calibration to the ResNet20 pre-trained image classifier on the CIFAR-10 data set are not consistent with the results obtained on tabular data sets. Figure 8(a) shows the Brier scores (lower is better) for the ResNet20 pre-trained image classifier on the CIFAR-10 data set. Note that HH was quite low, so the difference in performance between SWC and SWC-HH was small. In this case, temperature scaling out-performed similarity-based calibration methods.

Investigating these results led to the identification of a necessary condition for similarity-based calibration to improve on \hat{p} : the features used to compute similarity must be more informative about the (true but unobserved) data labels than about \hat{p} . Given two items x_i and x_j , let $s_F(i, j)$ be their similarity in (augmented) feature space X^+ , $s_P(i, j)$ be their similarity in probability space Δ_{K-1} , and $s_L(i, j)$ be their similarity in label space

2. Pre-trained models were obtained from <https://github.com/chenyaofo/pytorch-cifar-models>

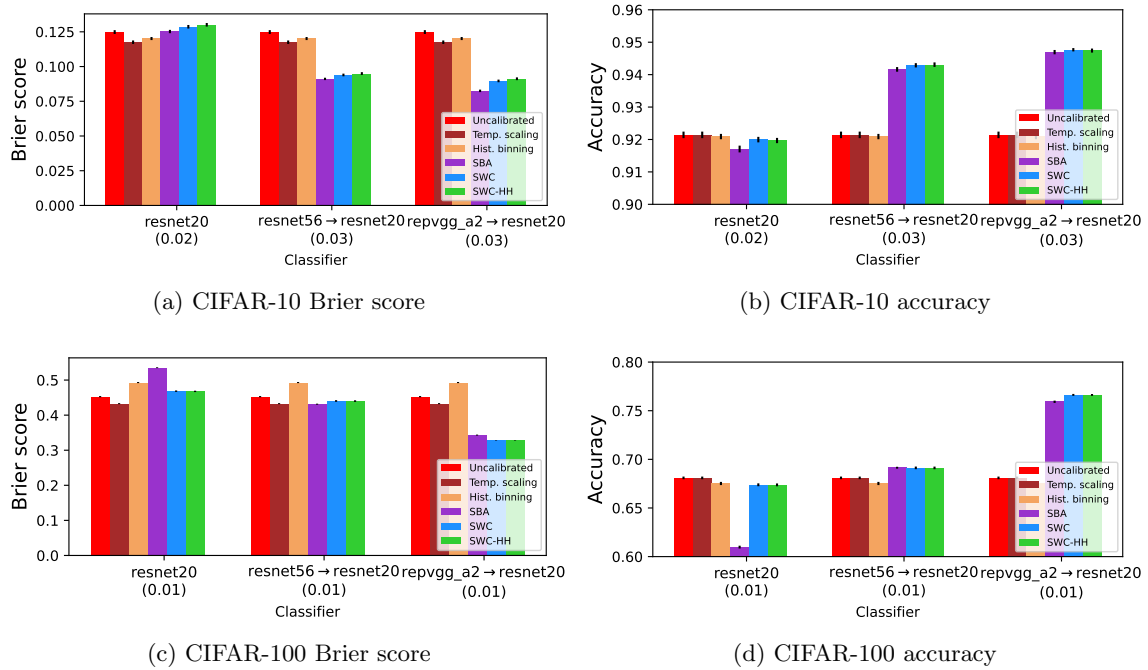


Figure 8: Calibration performance on CIFAR-10 (top) and CIFAR-100 (bottom row) using the ResNet20 pre-trained neural network over 10 trials (error bars show standard error). $\text{resnet56} \rightarrow \text{resnet20}$ and $\text{repvgg_a2} \rightarrow \text{resnet20}$ show results of using representations learned by other networks to calibrate ResNet20 predictions.

Table 1: Comparison of Brier scores for convolutional neural networks (lower is better; averaged over 10 trials with standard error in parentheses).

Data set	Uncal. ResNet20	Uncal. ResNet56	SWC ResNet56→ResNet20
CIFAR-10	0.1248 (0.001)	0.0959 (0.001)	0.0939 (0.001)
CIFAR-100	0.4527 (0.002)	0.4210 (0.002)	0.4404 (0.002)
Data set	Uncal. ResNet20	Uncal. RepVGG_A2	SWC RepVGG_A2→ResNet20
CIFAR-10	0.1248 (0.001)	0.0860 (0.001)	0.0896 (0.001)
CIFAR-100	0.4527 (0.002)	0.3267 (0.001)	0.3281 (0.001)

$[0, 1]$. We use RFprox as the similarity in feature space, Hellinger similarity (defined as $1 - H(\hat{p}_i, \hat{p}_j)$) as the similarity in probability space, and Hamming similarity (defined as $1 - d_H(y_i, y_j)$) as the similarity in label space. We compute $\rho_P = \text{corr}(s_F(t, c), s_P(t, c))$ and $\rho_L = \text{corr}(s_F(t, c), s_L(t, c))$ for $t \in X_{\text{test}}, c \in X_{\text{cal}}$ to quantify the relationship between similarity in feature space and probability space versus labels.

We found that when $\rho_L > \rho_P$, similarity-based calibration is beneficial. For example, for the “mnist-4v9” data set and the random forest classifier (using 1000 calibration and 500 test items), $\rho_L = 0.774 > \rho_P = 0.754$, and SWC achieved modest gains. For the same data set with the Naive Bayes classifier, $\rho_L = 0.644 > \rho_P = 0.315$, and SWC yielded dramatic gains. For CIFAR-10 with ResNet20 (using 5000 calibration and 5000 test items), we found that $\rho_L = 0.806 < \rho_P = 0.881$, and SWC did not yield an improvement.

We therefore also investigated whether representations learned by other models for the same data could yield a higher ρ_L and enable more effective similarity-based calibration. Figure 8 also shows results for calibrating resnet20 predictions in which the RFprox similarity measure is learned using the representations from ResNet56 ($\rho_L = 0.865$) or RepVGG_A2 ($\rho_L = 0.888$). These representations provide complementary information and enable large improvements in Brier score (reduced by 34%) and accuracy (increased by 2.5 percentage points). These results are consistent with the findings of Kalmady et al. (2021) in which a learned representation tailored for medical concepts (Med2Vec) improved the (inherent) calibration of rehospitalization and mortality predictions.

Note that the resulting cross-calibrated \hat{q} values are not the same as replacing ResNet20 predictions with ResNet56 or RepVGG_A2 predictions (see Table 1). Sometimes the uncalibrated predictions of the more complex network out-performed the cross-calibrated ResNet20 values, and in other cases the reverse was true. In all cases, calibrating ResNet20 with another network’s representation out-performed its uncalibrated \hat{p} . See Table 10 in Appendix A for the complete numeric values plotted in Figure 8.

As with the “fashion-mnist” data set, we found that SWC-HH achieved the best accuracy but not the best Brier score (Figure 8(b)). In fact, the similarity-based SBA method obtained the best Brier score. SWC’s performance was between these two values (although the difference between the three similarity-based methods was small).

The CIFAR-100 results are shown in Figure 8(c, d). HH values were extremely low. Temperature scaling yielded a small improvement in Brier score for ResNet20 predictions, but similarity-based methods did better when using the ResNet56 representation. For ResNet20, $\rho_L = 0.590$ which was much less than $\rho_P = 0.729$. The RepVGG_A2 latent representation ($\rho_L = 0.702 > \rho_P = 0.652$) enabled dramatic improvements, including a

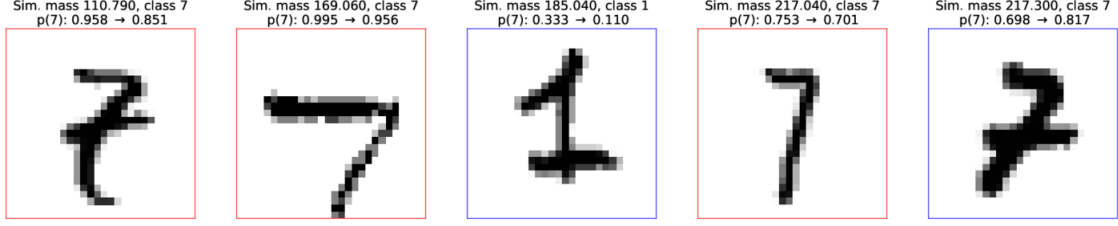


Figure 9: Test items from “mnist-1v7” with the lowest similarity mass for a linear SVM classifier. Items framed in blue (red) indicate whether SWC calibration helped (hurt).

reduction in Brier score of 28% and increase in accuracy of 9 percentage points (from 68% to 77%) (see Table 11).

7.2.4 SIMILARITY MASS HIGHLIGHTS CALIBRATION DATA GAPS AND DOMAIN SHIFT

Calibration with SWC or SWC-HH offers another benefit not provided by global methods such as Platt or temperature scaling. Because each item is individually calibrated by SWC, it is possible to report how much relevant calibration data was incorporated into the calibration of that item. We define the *similarity mass* M for item t that informs $\Phi(\hat{p}|t)$ as the sum of similarity weights for items drawn from calibration set C :

$$M_{t,C} = \sum_i s(t,i), x_i \in C. \quad (10)$$

Identifying items with low values for $M_{t,C}$ can draw attention to observations that are not well represented by the calibration set. These could be individual outliers or, if there is a large number of such items, they could be the result of domain shift between the calibration and test sets. Low $M_{t,C}$ values signal the need for more data (or more representative data) to be added to C . While previous studies focus solely on calibration performance as a function of the total calibration set *size*, similarity-based calibration can characterize the *relevance* of the calibration set to individual test items.

Figure 9 shows the five test items (of 500 total) with the lowest similarity mass after training a linear SVM on 500 MNIST “1” and “7” digits and calibrating with 3000 digits. Calibration with SWC was beneficial ($\hat{q}[y]$ increased for the true label y) for two of the five and detrimental ($\hat{q}[y]$ decreased) for three of them. These items are not necessarily ambiguous, but because they have less representation in the calibration set, the output \hat{q} may be less reliable.

Likewise, similarity mass can provide a warning when domain shift is present. We simulated domain shift (covariate shift) by rotating a subset of the test items 90 degrees counter-clockwise. Figure 10(a) shows the distribution of similarity mass values without any rotation; the peak value is around 900 and items with low similarity mass are rare. With 10% of the test set rotated (Figure 10(b)), the overall histogram changes a little, and the rotated items (orange bars) tend to have low similarity mass, signaling a need for inspection. With 50% (partial domain shift) rotated (Figure 10(c)), distinct populations for the rotated and unrotated items are clear, and with 100% rotated (complete domain shift), the whole histogram shifts to lower values (peak around 300).

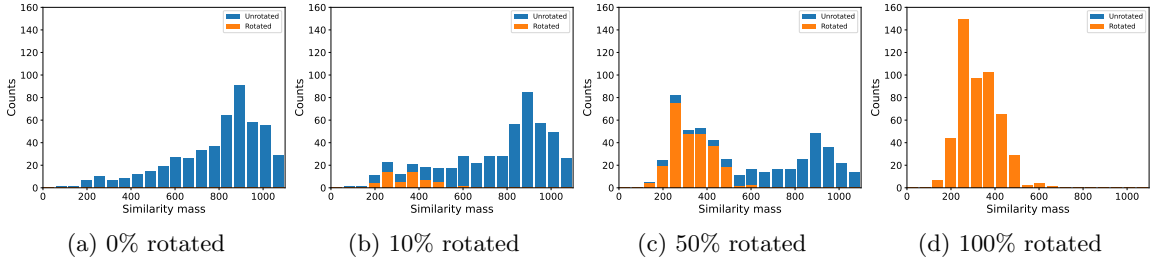


Figure 10: Distribution of similarity mass values for 500 test items (“mnist-1v7”) classified by a linear SVM with progressively more of the test set items rotated. Bar plots are stacked.

This result suggests that in a deployment setting, it is useful to monitor the similarity mass values that are reported by SWC. Knowledge about typical similarity mass values (or better, their distribution) could enable early detection of domain shift when new items originate from a changed distribution. That signal indicates that the calibration set, and likely the trained model as well, require revision. Platt, temperature scaling, histogram binning, and other methods provide a fixed mapping $\Phi(\hat{p})$ without regard to the item being calibrated; there is no signal to indicate whether Φ is still relevant. SWC uniquely provides an intrinsic measure of calibration set relevance through the similarity mass values obtained by each new item.

8. Conclusions, limitations, and future work

In this work, we explored the benefits of local, individual calibration for each item, in contrast to widely used global classifier calibration methods. We identified hidden heterogeneity as a strong indicator of the need for local calibration, when there are subpopulations within a data set that have the same uncalibrated predicted probability \hat{p} yet require diverse corrections to achieve a well calibrated probability \hat{q} . Experiments with tabular data sets and diverse machine learning classifiers indicate that local calibration improves Brier score in proportion to the average hidden heterogeneity (HH) value in the data set. We highlight this finding as an important step towards not only correcting miscalibration but also explaining and understanding it. When HH is very low, global methods such as temperature scaling are sufficient, but otherwise, local calibration is preferred.

We proposed a similarity-based approach to local calibration (SWC) that weights evidence from the calibration set according to its similarity to the test item in augmented feature space. This concept builds on prior work with Similarity-Binning Averaging (SBA), which calibrates (without weighting) using the 10 nearest neighbors based on Euclidean distance in augmented feature space (Bella et al., 2009). In most cases, we found that SWC out-performs SBA. Additional benefits can be obtained by incorporating HH directly into the SWC algorithm (SWC-HH). For neural networks, the latent representation learned by the model is often strongly correlated with its output \hat{p} values. We found that this limits the ability of similarity-based calibration to improve over \hat{p} . Leveraging the representation learned by another network with a higher ρ_L value can yield benefits for calibration. A final and unique benefit of similarity-based calibration is that the explicit characterization

of similarity mass can serve to warn when a given test item lacks good representation in the calibration set, including the presence of domain shift.

Runtime. The computational cost of local calibration methods tends to be higher than that of global methods, since each item is independently modeled rather than constructing a single model to apply to all items. However, this also means that calibration can be conducted lazily, as needed, given a similarity measure. The computation of hidden heterogeneity requires (1) the identification of an item’s nearest neighbors in the probability simplex Δ_{K-1} , which can be costly with a large number of classes, and (2) training a specialized classifier to estimate the potential Brier score improvement (Equation 7). The choice of classifier type influences the total runtime.

Preservation of accuracy. SWC and SWC-HH are not rank-preserving calibration methods. This means that in addition to modifying the calibration properties of the predictions, they can also change the predicted class and therefore the accuracy of predictions. We have seen that this is a benefit of local calibration. Temperature scaling, in contrast, does preserve rank and accuracy, because without a bias term it cannot move items to the other side of the decision threshold. Some researchers favor rank-preserving methods (Zhang et al., 2020; Patel et al., 2021), since they seek to improve calibration without sacrificing accuracy. However, this constraint also prevents them from increasing accuracy, which is an option available to Platt scaling, histogram binning, SWC, etc. On the whole, we agree with Bella et al. (2013) that there is no need to preserve item rankings given the opportunity to improve both accuracy and calibration. However, we acknowledge that in some applications, there could be a need to choose a rank-preserving calibration method to ensure accuracy is unchanged (up or down) for user acceptance.

Future work. There are several important directions for future work. It is possible that within the same data set, some items are best calibrated with global methods while others (where HH is present) benefit from local calibration. A hybrid method that selectively applies global/local calibration, or some combination of the two, for each test item could potentially out-perform either one. In addition, SWC is well designed to naturally accommodate domain shift, if the calibration data set is drawn from the shifted distribution. Sampling bias in the training set, whether intentional or not, induces a particular kind of domain shift that is especially important to address to meet fairness goals when predictions are made in a deployment setting. We plan to explore these directions in the future.

Acknowledgments

This material is based upon work supported by the Defense Advanced Research Projects Agency (DARPA) under Contract No. HR001119C0112. Any opinions, findings and conclusions or recommendations expressed in this material are those of the authors and do not necessarily reflect the views of the DARPA.

References

Amr M. Alexandari, Anshul Kundaje, and Avanti Shrikumar. Maximum likelihood with bias-corrected calibration is hard-to-beat at label shift adaptation. In *Proceedings of the 37th International Conference on Machine Learning*, pages 222–232, 2020.

Antonio Bella, Cèsar Ferri, José Hernández-Orallo, and María José Ramírez-Quintana. Similarity-binning averaging: A generalisation of binning calibration. In *Intelligent Data Engineering and Automated Learning - IDEAL 2009, Lecture Notes in Computer Science*, volume 5788, pages 341–349, 2009.

Antonio Bella, Cèsar Ferri, José Hernández-Orallo, and María José Ramírez-Quintana. On the effect of calibration in classifier combination. *Applied Intelligence*, 38:566–585, 2013.

Leo Breiman. Random forests. *Machine Learning*, 45:5–32, 2001.

Leo Breiman, Jerome H. Friedman, R. A. Olshen, and Charles J. Stone. *Classification and regression trees*. Chapman and Hall, New York, NY, 1984.

Glenn W. Brier. Verification of forecasts expressed in terms of probability. *Monthly Weather Review*, 78(1):1–3, 1950. doi: 10.1175/1520-0493(1950)078<0001:VOFEIT>2.0.CO;2.

Jochen Bröcker. Estimating reliability and resolution of probability forecasts through decomposition of the empirical score. *Climate Dynamics*, 39:655–667, 2011.

Adele Cutler, D. Richard Cutler, and John R. Stevens. *Ensemble machine learning: Methods and applications*, chapter Random forests. Springer, 2012.

Xiaohan Ding, Xiangyu Zhang, Ningning Ma, Jungong Han, Guiguang Ding, and Jian Sun. RepVGG: Making VGG-style ConvNets great again. In *Proceedings of the IEEE/CVF Conference on Computer Vision and Pattern Recognition (CVPR)*, pages 13733–13742, Jun 2021.

Shohei Enomoto and Takeharu Eda. Learning to cascade: Confidence calibration for improving the accuracy and computational cost of cascade inference systems. In *Proceedings of the AAAI Conference on Artificial Intelligence*, volume 35(8), pages 7331–7339, 2021.

C. A. T. Ferro and T. E. Fricker. A bias-corrected decomposition of the Brier score. *Quarterly Journal of the Royal Meteorological Society*, 138(668):1954–1960, 2012.

Chuan Guo, Geoff Pleiss, Yu Sun, and Kilian Q. Weinberger. On calibration of modern neural networks. In *Proceedings of the 34th International Conference on Machine Learning*, pages 1321–1330, 2017. doi: 10.5555/3305381.3305518.

Trevor Hastie, Robert Tibshirani, and Jerome Friedman. *The Elements of Statistical Learning: Data Mining, Inference, and Prediction*. Springer, 2nd edition, 2009.

Kaiming He, Xiangyu Zhang, Shaoqing Ren, and Jian Sun. Deep residual learning for image recognition. In *Proceedings of the IEEE Conference on Computer Vision and Pattern Recognition (CVPR)*, pages 770–778, 2016.

Sunil Kalmady, Weijie Sun, Justin Ezekowitz, Nowell Fine, Jonathan Howlett, Anamaria Savu, Russ Greiner, and Padma Kaul. Improving the calibration of long term predictions of heart failure rehospitalizations using medical concept embedding. In *Proceedings of AAAI Spring Symposium on Survival Prediction - Algorithms, Challenges, and Applications*, volume 146 of *PMLR*, pages 70–82, 2021.

Alex Krizhevsky. Learning multiple layers of features from tiny images. Technical report, University of Toronto, 2009.

Kriste Krstovski, David A. Smith, Hanna M. Wallach, and Andrew McGregor. Efficient nearest-neighbor search in the probability simplex. In *Proceedings of the 2013 Conference on the Theory of Information Retrieval*, pages 101–108, 2013. doi: 10.1145/2499178.2499189.

Meelis Kull, Telmo M. Silva Filho, and Peter Flach. Beyond sigmoids: How to obtain well-calibrated probabilities from binary classifiers with beta calibration. *Electronic Journal of Statistics*, 11:5052–5080, 2017.

Meelis Kull, Miquel Perello-Nieto, Markus Kängsepp, Telmo Silva Filho, Hao Song, and Peter Flach. Obtaining well-calibrated multiclass probabilities with Dirichlet calibration. In *Proceedings of the 33rd Conference on Neural Information Processing Systems (NeurIPS)*, 2019.

Ananya Kumar, Percy Liang, and Tengyu Ma. Verified uncertainty calibration. In *Proceedings of the 33rd Conference on Neural Information Processing Systems*, 2019.

Aviral Kumar, Sunita Sarawagi, and Ujjwal Jain. Trainable calibration measures for neural networks from kernel mean embeddings. In *Proceedings of the 35th International Conference on Machine Learning*, 2018.

Yann LeCun, Corinna Cortes, and Christopher J. C. Burges. <http://yann.lecun.com/exdb/mnist/>, 2010.

Rachel Luo, Aadyot Bhatnagar, Yu Bai, Shengjia Zhao, Huan Wang, Caiming Xiong, Silvio Savarese, Stefano Ermon, Edward Schmerling, and Marco Pavone. Localized calibration: Metrics and recalibration. arXiv, version as of December 15, 2021, unpublished. URL <https://arxiv.org/abs/2102.10809>.

Matthias Minderer, Josip Djolonga, Rob Romijnders, Frances Hubis, Xiaohua Zhai, Neil Houlsby, Dustin Tran, and Mario Lucic. Revisiting the calibration of modern neural networks. In *Proceedings of the 35th Conference on Neural Information Processing Systems (NeurIPS)*, 2021.

Jishnu Mukhoti, Viveka Kulharia, Amartya Sanyal, Stuart Golodetz, Philip H.S. Torr, and Puneet K. Dokania. Calibrating deep neural networks using focal loss. In *Proceedings of the 34th Conference on Neural Information Processing Systems (NeurIPS)*, 2020.

Mahdi Pakdaman Naeini, Gregory F Cooper, and Milos Hauskrecht. Obtaining well calibrated probabilities using Bayesian binning. In *Proceedings of the Twenty-Ninth AAAI Conference on Artificial Intelligence*, pages 2901–2907, 2015.

Alexandru Niculescu-Mizil and Rich Caruana. Predicting good probabilities with supervised learning. In *Proceedings of the 22nd International Conference on Machine Learning*, pages 625–632, 2005.

Jeremy Nixon, Michael W. Dusenberry, Linchuan Zhang, Ghassen Jerfel, and Dustin Tran. Measuring calibration in deep learning. In *Proceedings of the IEEE/CVF Conference on Computer Vision and Pattern Recognition (CVPR) Workshops*, pages 38–41, 2019.

Yaniv Ovadia, Emily Fertig, Jie Ren, Zachary Nado, D Sculley, Sebastian Nowozin, Joshua V. Dillon, Balaji Lakshminarayanan, and Jasper Snoek. Can you trust your model’s uncertainty? Evaluating predictive uncertainty under dataset shift. In *Proceedings of the 33rd Conference on Neural Information Processing Systems (NeurIPS)*, 2019.

Kanil Patel, William Beluch, Bin Yang, Michael Pfeiffer, and Dan Zhang. Multi-class uncertainty calibration via mutual information maximization-based binning. In *Proceedings of the International Conference on Learning Representations (ICLR)*, 2021.

F. Pedregosa, G. Varoquaux, A. Gramfort, V. Michel, B. Thirion, O. Grisel, M. Blondel, P. Prettenhofer, R. Weiss, V. Dubourg, J. Vanderplas, A. Passos, D. Cournapeau, M. Brucher, M. Perrot, and E. Duchesnay. Scikit-learn: Machine learning in Python. *Journal of Machine Learning Research*, 12:2825–2830, 2011.

John Platt. Probabilistic outputs for support vector machines and comparisons to regularized likelihood methods. *Advances in Large Margin Classifiers*, 10(3):61–74, 1999.

Erwan Scornet. Random forests and kernel methods. *IEEE Transactions on Information Theory*, 62(3):1485–1500, 2016.

Seonguk Seo, Paul Hongsuck Seo, and Bohyung Han. Learning for single-shot confidence calibration in deep neural networks through stochastic inferences. In *Proceedings of the IEEE/CVF Conference on Computer Vision and Pattern Recognition (CVPR)*, pages 9030–9038, 2019.

Christian Tomani and Florian Buettnner. Towards trustworthy predictions from deep neural networks with fast adversarial calibration. In *Proceedings of the AAAI Conference on Artificial Intelligence*, volume 35(11), pages 9886–9896, 2021.

Juozas Vaicenavicius, David Widmann, Carl Andersson, Fredrik Lindsten, Jacob Roll, and Thomas B. Schön. Evaluating model calibration in classification. In *Proceedings of the 22nd International Conference on Artificial Intelligence and Statistics (AISTATS)*, 2019.

David Widmann, Fredrik Lindsten, and Dave Zachariah. Calibration tests in multi-class classification: A unifying framework. In *Proceedings of the 33rd Conference on Neural Information Processing Systems (NeurIPS)*, 2019.

Han Xiao, Kashif Rasul, and Roland Vollgraf. Fashion-MNIST: a novel image dataset for benchmarking machine learning algorithms. arXiv, version as of August 28, 2017, unpublished. URL <https://arxiv.org/abs/2102.10809>.

Bianca Zadrozny and Charles Elkan. Obtaining calibrated probability estimates from decision trees and naive Bayesian classifiers. In *Proceedings of the International Conference on Machine Learning*, pages 609–616, 2001.

Bianca Zadrozny and Charles Elkan. Transforming classifier scores into accurate multiclass probability estimates. In *Proceedings of the ACM SIGKDD International Conference on Knowledge Discovery and Data Mining*, pages 694–699, 2002.

Jize Zhang, Bhavya Kailkhura, and T. Yong-Jin Han. Mix-n-match : Ensemble and compositional methods for uncertainty calibration in deep learning. In *Proceedings of the 37th International Conference on Machine Learning*, pages 11117–11128, 2020.

Shengjia Zhao, Tengyu Ma, and Stefano Ermon. Individual calibration with randomized forecasting. In *Proceedings of the 37th International Conference on Machine Learning*, pages 11387–11397, 2020.

Appendix A. Numeric experimental results

In this appendix, we provide numeric tables with the Brier scores and accuracy values obtained for all binary and multi-class data sets employed in this study. In each table, models (rows) are ordered by the uncalibrated model's performance (high to low for Brier score, low to high for accuracy).

Table 2: Results for mnist-4v9 ($n_{cal} = 3000$, 10 trials). The best result(s) for each model (within 1 standard error) are in bold.

Brier score						
Model	Uncal.	Platt	Hist bin	SBA	SWC	SWC-HH
NB	0.4765 (0.019)	0.3403 (0.009)	0.2705 (0.009)	0.0668 (0.004)	0.0481 (0.004)	0.0317 (0.004)
DT	0.1631 (0.005)	0.1590 (0.004)	0.1648 (0.004)	0.0655 (0.005)	0.0528 (0.004)	0.0428 (0.004)
RF	0.0944 (0.003)	0.0492 (0.005)	0.0511 (0.005)	0.0661 (0.005)	0.0421 (0.004)	0.0368 (0.004)
SVM	0.0880 (0.008)	0.0884 (0.008)	0.0873 (0.008)	0.0657 (0.005)	0.0455 (0.005)	0.0374 (0.004)
RBFSVM	0.0856 (0.008)	0.0927 (0.009)	0.0772 (0.007)	0.0657 (0.005)	0.0418 (0.006)	0.0349 (0.004)
GBT	0.0682 (0.005)	0.0720 (0.005)	0.0609 (0.004)	0.0652 (0.005)	0.0447 (0.005)	0.0422 (0.006)

Accuracy						
Model	Uncal.	Platt	Hist bin	SBA	SWC	SWC-HH
NB	0.7616 (0.010)	0.7618 (0.010)	0.8628 (0.010)	0.9594 (0.003)	0.9688 (0.003)	0.9822 (0.003)
DT	0.8998 (0.003)	0.9004 (0.003)	0.8984 (0.003)	0.9610 (0.004)	0.9634 (0.002)	0.9738 (0.002)
RBFSVM	0.9404 (0.005)	0.9410 (0.005)	0.9444 (0.006)	0.9604 (0.003)	0.9722 (0.004)	0.9812 (0.002)
SVM	0.9454 (0.005)	0.9460 (0.005)	0.9476 (0.005)	0.9602 (0.003)	0.9682 (0.003)	0.9766 (0.002)
GBT	0.9568 (0.002)	0.9568 (0.002)	0.9596 (0.003)	0.9612 (0.003)	0.9710 (0.004)	0.9762 (0.003)
RF	0.9680 (0.003)	0.9684 (0.004)	0.9684 (0.003)	0.9598 (0.003)	0.9748 (0.003)	0.9806 (0.002)

Table 3: Results for mnist-1v7 ($n_{cal} = 3000$, 10 trials). The best result(s) for each model (within 1 standard error) are in bold.

Brier score						
Model	Uncal.	Platt	Hist bin	SBA	SWC	SWC-HH
DT	0.0657 (0.005)	0.0657 (0.005)	0.0905 (0.007)	0.0188 (0.002)	0.0177 (0.002)	0.0165 (0.002)
RBFSVM	0.0484 (0.003)	0.0519 (0.003)	0.0367 (0.002)	0.0188 (0.002)	0.0154 (0.002)	0.0127 (0.002)
NB	0.0419 (0.004)	0.0411 (0.004)	0.0403 (0.004)	0.0186 (0.002)	0.0127 (0.002)	0.0130 (0.002)
GBT	0.0419 (0.005)	0.0419 (0.005)	0.0323 (0.003)	0.0187 (0.002)	0.0165 (0.002)	0.0162 (0.002)
RF	0.0230 (0.002)	0.0155 (0.002)	0.0161 (0.002)	0.0187 (0.002)	0.0147 (0.002)	0.0127 (0.002)
SVM	0.0170 (0.002)	0.0165 (0.002)	0.0165 (0.002)	0.0186 (0.002)	0.0136 (0.002)	0.0127 (0.002)

Accuracy						
Model	Uncal.	Platt	Hist bin	SBA	SWC	SWC-HH
DT	0.9606 (0.003)	0.9600 (0.003)	0.9550 (0.004)	0.9870 (0.001)	0.9876 (0.002)	0.9894 (0.002)
RBFSVM	0.9690 (0.002)	0.9692 (0.002)	0.9722 (0.002)	0.9870 (0.001)	0.9900 (0.002)	0.9932 (0.001)
GBT	0.9774 (0.003)	0.9778 (0.003)	0.9800 (0.002)	0.9870 (0.001)	0.9890 (0.001)	0.9892 (0.001)
NB	0.9790 (0.002)	0.9790 (0.002)	0.9798 (0.003)	0.9870 (0.001)	0.9920 (0.001)	0.9918 (0.001)
RF	0.9898 (0.002)	0.9898 (0.002)	0.9902 (0.002)	0.9870 (0.001)	0.9902 (0.001)	0.9930 (0.001)
SVM	0.9900 (0.001)	0.9900 (0.001)	0.9894 (0.001)	0.9870 (0.001)	0.9906 (0.001)	0.9924 (0.001)

Table 4: Results for mnist-3v8 ($n_{cal} = 3000$, 10 trials). The best result(s) for each model (within 1 standard error) are in bold.

Brier score						
Model	Uncal.	Platt	Hist bin	SBA	SWC	SWC-HH
NB	0.5341 (0.029)	0.3651 (0.012)	0.2502 (0.011)	0.0501 (0.004)	0.0563 (0.004)	0.0335 (0.004)
DT	0.1459 (0.010)	0.1448 (0.009)	0.1451 (0.010)	0.0496 (0.004)	0.0564 (0.005)	0.0434 (0.004)
RF	0.0952 (0.003)	0.0625 (0.005)	0.0646 (0.005)	0.0497 (0.004)	0.0520 (0.004)	0.0333 (0.003)
SVM	0.0845 (0.005)	0.0842 (0.005)	0.0832 (0.004)	0.0495 (0.004)	0.0503 (0.004)	0.0388 (0.003)
RBFSVM	0.0753 (0.003)	0.0778 (0.004)	0.0677 (0.004)	0.0493 (0.004)	0.0446 (0.003)	0.0334 (0.003)
GBT	0.0671 (0.007)	0.0698 (0.007)	0.0628 (0.006)	0.0493 (0.004)	0.0515 (0.005)	0.0394 (0.004)
Accuracy						
Model	Uncal.	Platt	Hist bin	SBA	SWC	SWC-HH
NB	0.7326 (0.014)	0.7326 (0.014)	0.9020 (0.008)	0.9672 (0.004)	0.9638 (0.003)	0.9814 (0.002)
DT	0.9036 (0.006)	0.9084 (0.007)	0.9106 (0.005)	0.9678 (0.004)	0.9632 (0.003)	0.9746 (0.003)
RBFSVM	0.9470 (0.003)	0.9466 (0.003)	0.9532 (0.003)	0.9682 (0.004)	0.9708 (0.002)	0.9822 (0.002)
SVM	0.9472 (0.003)	0.9474 (0.003)	0.9498 (0.003)	0.9680 (0.004)	0.9660 (0.003)	0.9766 (0.002)
GBT	0.9590 (0.004)	0.9596 (0.004)	0.9570 (0.004)	0.9684 (0.004)	0.9660 (0.003)	0.9778 (0.002)
RF	0.9596 (0.004)	0.9598 (0.003)	0.9594 (0.003)	0.9682 (0.004)	0.9670 (0.003)	0.9814 (0.002)

Table 5: Results for mnist-3v5 ($n_{cal} = 3000$, 10 trials). The best result(s) for each model (within 1 standard error) are in bold.

Brier score						
Model	Uncal.	Platt	Hist bin	SBA	SWC	SWC-HH
NB	0.5127 (0.037)	0.3557 (0.014)	0.2656 (0.009)	0.0576 (0.004)	0.0444 (0.003)	0.0247 (0.003)
DT	0.2188 (0.006)	0.2107 (0.006)	0.2127 (0.006)	0.0568 (0.004)	0.0450 (0.003)	0.0288 (0.003)
SVM	0.0988 (0.005)	0.0993 (0.005)	0.0999 (0.005)	0.0570 (0.004)	0.0452 (0.003)	0.0353 (0.003)
RF	0.0973 (0.002)	0.0485 (0.004)	0.0500 (0.004)	0.0570 (0.004)	0.0375 (0.004)	0.0304 (0.006)
RBFSVM	0.0740 (0.003)	0.0774 (0.005)	0.0724 (0.003)	0.0565 (0.004)	0.0367 (0.003)	0.0259 (0.004)
GBT	0.0591 (0.003)	0.0630 (0.004)	0.0558 (0.003)	0.0561 (0.004)	0.0385 (0.003)	0.0316 (0.005)
Accuracy						
Model	Uncal.	Platt	Hist bin	SBA	SWC	SWC-HH
NB	0.7426 (0.018)	0.7438 (0.018)	0.8594 (0.006)	0.9624 (0.004)	0.9720 (0.002)	0.9854 (0.002)
DT	0.8612 (0.003)	0.8622 (0.003)	0.8616 (0.004)	0.9638 (0.004)	0.9714 (0.002)	0.9832 (0.002)
SVM	0.9364 (0.003)	0.9364 (0.004)	0.9342 (0.003)	0.9634 (0.004)	0.9692 (0.003)	0.9778 (0.002)
RBFSVM	0.9446 (0.004)	0.9446 (0.004)	0.9484 (0.002)	0.9638 (0.004)	0.9744 (0.002)	0.9868 (0.002)
GBT	0.9604 (0.002)	0.9614 (0.002)	0.9612 (0.003)	0.9642 (0.004)	0.9728 (0.002)	0.9820 (0.002)
RF	0.9666 (0.004)	0.9664 (0.003)	0.9656 (0.003)	0.9634 (0.004)	0.9752 (0.003)	0.9830 (0.003)

Table 6: Results for moons ($n_{cal} = 3000$, 10 trials). The best result(s) for each model (within 1 standard error) are in bold.

Brier score						
Model	Uncal.	Platt	Hist bin	SBA	SWC	SWC-HH
NB	0.2178 (0.007)	0.2233 (0.007)	0.2214 (0.006)	0.1317 (0.003)	0.1332 (0.004)	0.1396 (0.004)
SVM	0.2131 (0.006)	0.2184 (0.007)	0.2203 (0.006)	0.1315 (0.002)	0.1336 (0.003)	0.1400 (0.004)
DT	0.1586 (0.006)	0.1590 (0.006)	0.1538 (0.006)	0.1302 (0.003)	0.1324 (0.003)	0.1366 (0.003)
GBT	0.1469 (0.005)	0.1500 (0.005)	0.1465 (0.004)	0.1277 (0.003)	0.1307 (0.003)	0.1374 (0.004)
RF	0.1410 (0.005)	0.1421 (0.005)	0.1456 (0.005)	0.1291 (0.003)	0.1330 (0.004)	0.1367 (0.004)
RBFSVM	0.1371 (0.005)	0.1416 (0.005)	0.1400 (0.004)	0.1302 (0.003)	0.1302 (0.003)	0.1339 (0.003)

Accuracy						
Model	Uncal.	Platt	Hist bin	SBA	SWC	SWC-HH
NB	0.8462 (0.005)	0.8460 (0.005)	0.8440 (0.004)	0.9132 (0.004)	0.9144 (0.003)	0.9130 (0.003)
SVM	0.8480 (0.006)	0.8478 (0.005)	0.8448 (0.005)	0.9142 (0.004)	0.9140 (0.002)	0.9132 (0.003)
DT	0.8964 (0.005)	0.8964 (0.005)	0.8994 (0.005)	0.9136 (0.003)	0.9152 (0.002)	0.9138 (0.003)
GBT	0.9010 (0.004)	0.9024 (0.004)	0.9026 (0.004)	0.9152 (0.003)	0.9178 (0.003)	0.9130 (0.003)
RF	0.9062 (0.004)	0.9066 (0.004)	0.9024 (0.003)	0.9144 (0.003)	0.9134 (0.003)	0.9134 (0.003)
RBFSVM	0.9064 (0.003)	0.9052 (0.003)	0.9028 (0.003)	0.9162 (0.003)	0.9150 (0.003)	0.9142 (0.003)

Table 7: Results for letter ($n_{cal} = 5000$, 10 trials). The best result(s) for each model (within 1 standard error) are in bold.

Brier score						
Model	Uncal.	TS	Hist bin	SBA	SWC	SWC-HH
NB	0.5354 (0.006)	0.5084 (0.005)	0.4902 (0.005)	0.2070 (0.004)	0.2329 (0.004)	0.2248 (0.004)
DT	0.5035 (0.005)	0.5273 (0.005)	0.7212 (0.006)	0.2013 (0.004)	0.2251 (0.005)	0.2236 (0.006)
SVM	0.3268 (0.003)	0.2612 (0.004)	0.2764 (0.004)	0.1936 (0.003)	0.1953 (0.003)	0.1947 (0.003)
RF	0.2503 (0.003)	0.1718 (0.004)	0.1935 (0.004)	0.1853 (0.003)	0.1418 (0.004)	0.1418 (0.004)
RBFSVM	0.2465 (0.004)	0.2166 (0.005)	0.2265 (0.004)	0.1851 (0.003)	0.1748 (0.004)	0.1739 (0.004)
GBT	0.2157 (0.003)	0.2062 (0.002)	0.2145 (0.003)	0.1612 (0.003)	0.1854 (0.004)	0.1831 (0.004)

Accuracy						
Model	Uncal.	TS	Hist bin	SBA	SWC	SWC-HH
DT	0.6247 (0.005)	0.6247 (0.005)	0.5100 (0.007)	0.8675 (0.004)	0.8450 (0.004)	0.8828 (0.003)
NB	0.6294 (0.004)	0.6294 (0.004)	0.6487 (0.005)	0.8617 (0.003)	0.8394 (0.003)	0.8496 (0.003)
SVM	0.8234 (0.003)	0.8234 (0.003)	0.8206 (0.002)	0.8747 (0.003)	0.8705 (0.001)	0.8711 (0.001)
RBFSVM	0.8457 (0.004)	0.8457 (0.004)	0.8461 (0.004)	0.8785 (0.003)	0.8833 (0.003)	0.8842 (0.003)
GBT	0.8556 (0.002)	0.8556 (0.002)	0.8533 (0.002)	0.8945 (0.003)	0.8783 (0.002)	0.8806 (0.002)
RF	0.8783 (0.003)	0.8783 (0.003)	0.8762 (0.003)	0.8788 (0.002)	0.9054 (0.002)	0.9054 (0.002)

Table 8: Results for mnist10 ($n_{cal} = 5000$, 10 trials). The best result(s) for each model (within 1 standard error) are in bold.

Brier score						
Model	Uncal.	TS	Hist bin	SBA	SWC	SWC-HH
NB	0.8134 (0.017)	0.7970 (0.017)	0.5799 (0.016)	0.1796 (0.002)	0.1609 (0.003)	0.1111 (0.003)
DT	0.5244 (0.010)	0.5323 (0.008)	0.5452 (0.008)	0.1789 (0.002)	0.1643 (0.003)	0.1164 (0.003)
RF	0.2995 (0.002)	0.1482 (0.003)	0.1602 (0.003)	0.1792 (0.002)	0.1286 (0.003)	0.1273 (0.003)
GBT	0.2157 (0.004)	0.2065 (0.003)	0.2049 (0.003)	0.1782 (0.002)	0.1449 (0.002)	0.1418 (0.003)
RBFSVM	0.1948 (0.004)	0.1869 (0.005)	0.1808 (0.004)	0.1784 (0.002)	0.1285 (0.003)	0.1248 (0.003)
SVM	0.1872 (0.005)	0.1743 (0.005)	0.1774 (0.004)	0.1786 (0.002)	0.1296 (0.003)	0.1273 (0.003)
Accuracy						
Model	Uncal.	TS	Hist bin	SBA	SWC	SWC-HH
NB	0.5923 (0.008)	0.5923 (0.008)	0.6098 (0.025)	0.8780 (0.002)	0.8996 (0.003)	0.9441 (0.001)
DT	0.6440 (0.008)	0.6440 (0.008)	0.6344 (0.008)	0.8788 (0.002)	0.8964 (0.004)	0.9407 (0.002)
GBT	0.8589 (0.003)	0.8589 (0.003)	0.8609 (0.003)	0.8792 (0.002)	0.9013 (0.002)	0.9076 (0.002)
RBFSVM	0.8664 (0.004)	0.8664 (0.004)	0.8760 (0.004)	0.8785 (0.003)	0.9162 (0.003)	0.9214 (0.002)
SVM	0.8847 (0.004)	0.8847 (0.004)	0.8839 (0.005)	0.8789 (0.003)	0.9159 (0.003)	0.9175 (0.003)
RF	0.8979 (0.003)	0.8979 (0.003)	0.9027 (0.003)	0.8783 (0.003)	0.9163 (0.003)	0.9173 (0.003)

Table 9: Results for fashion-mnist ($n_{cal} = 5000$, 10 trials). The best result(s) for each model (within 1 standard error) are in bold.

Brier score						
Model	Uncal.	TS	Hist bin	SBA	SWC	SWC-HH
NB	0.9365 (0.015)	0.9207 (0.015)	0.6359 (0.008)	0.2885 (0.006)	0.2548 (0.006)	0.3009 (0.012)
DT	0.5648 (0.011)	0.5563 (0.009)	0.6134 (0.008)	0.2881 (0.006)	0.2546 (0.006)	0.2938 (0.012)
GBT	0.4269 (0.009)	0.3636 (0.006)	0.3546 (0.006)	0.2879 (0.006)	0.2515 (0.006)	0.2848 (0.013)
RBFSVM	0.3464 (0.006)	0.3459 (0.006)	0.3382 (0.006)	0.2887 (0.006)	0.2524 (0.006)	0.2840 (0.011)
RF	0.3441 (0.005)	0.3139 (0.006)	0.3130 (0.007)	0.2883 (0.006)	0.2526 (0.007)	0.2735 (0.010)
SVM	0.3384 (0.006)	0.3272 (0.006)	0.3271 (0.007)	0.2887 (0.006)	0.2451 (0.006)	0.2652 (0.009)
Accuracy						
Model	Uncal.	TS	Hist bin	SBA	SWC	SWC-HH
NB	0.5314 (0.008)	0.5314 (0.008)	0.5670 (0.011)	0.7936 (0.004)	0.8204 (0.005)	0.8490 (0.006)
DT	0.6276 (0.010)	0.6276 (0.010)	0.5890 (0.008)	0.7962 (0.004)	0.8186 (0.005)	0.8502 (0.006)
GBT	0.7410 (0.006)	0.7410 (0.006)	0.7516 (0.006)	0.7972 (0.004)	0.8214 (0.004)	0.8386 (0.006)
RBFSVM	0.7512 (0.005)	0.7512 (0.005)	0.7568 (0.005)	0.7948 (0.005)	0.8248 (0.005)	0.8442 (0.006)
SVM	0.7720 (0.005)	0.7720 (0.005)	0.7776 (0.006)	0.7950 (0.005)	0.8288 (0.005)	0.8434 (0.005)
RF	0.7722 (0.006)	0.7722 (0.006)	0.7810 (0.008)	0.7950 (0.005)	0.8216 (0.005)	0.8298 (0.006)

Table 10: Results for CIFAR-10 ($n_{cal} = 5000$, 10 trials). The best result(s) for each model (within 1 standard error) are in bold. → indicates the use of a different representation to calibrate the previous model.

Brier score						
Model	Uncal.	TS	Hist bin	SBA	SWC	SWC-HH
resnet20	0.1248 (0.001)	0.1175 (0.001)	0.1202 (0.001)	0.1252 (0.001)	0.1286 (0.001)	0.1301 (0.001)
resnet56→	0.1248 (0.001)	0.1175 (0.001)	0.1202 (0.001)	0.0911 (0.001)	0.0939 (0.001)	0.0950 (0.001)
repvgg-a2→	0.1248 (0.001)	0.1175 (0.001)	0.1202 (0.001)	0.0825 (0.001)	0.0896 (0.001)	0.0912 (0.001)
resnet56	0.0959 (0.001)	0.0889 (0.001)	0.0925 (0.001)	0.0928 (0.001)	0.0986 (0.001)	0.1002 (0.001)
resnet20→	0.0959 (0.001)	0.0889 (0.001)	0.0925 (0.001)	0.1126 (0.001)	0.0939 (0.001)	0.0963 (0.001)
repvgg-a2→	0.0959 (0.001)	0.0889 (0.001)	0.0925 (0.001)	0.0824 (0.001)	0.0889 (0.001)	0.0904 (0.001)
repvgg-a2	0.0860 (0.001)	0.0798 (0.001)	0.0822 (0.001)	0.0825 (0.001)	0.0900 (0.001)	0.0911 (0.001)
resnet20→	0.0860 (0.001)	0.0798 (0.001)	0.0822 (0.001)	0.1103 (0.001)	0.0851 (0.001)	0.0873 (0.001)
resnet56→	0.0860 (0.001)	0.0798 (0.001)	0.0822 (0.001)	0.0880 (0.001)	0.0807 (0.001)	0.0830 (0.001)
Accuracy						
Model	Uncal.	TS	Hist bin	SBA	SWC	SWC-HH
resnet20	0.9214 (0.001)	0.9214 (0.001)	0.9209 (0.001)	0.9171 (0.001)	0.9200 (0.001)	0.9197 (0.001)
resnet56→	0.9214 (0.001)	0.9214 (0.001)	0.9209 (0.001)	0.9416 (0.001)	0.9429 (0.001)	0.9431 (0.001)
repvgg-a2→	0.9214 (0.001)	0.9214 (0.001)	0.9209 (0.001)	0.9469 (0.001)	0.9477 (0.001)	0.9474 (0.001)
resnet56	0.9432 (0.001)	0.9432 (0.001)	0.9413 (0.001)	0.9408 (0.001)	0.9407 (0.001)	0.9402 (0.001)
resnet20→	0.9432 (0.001)	0.9432 (0.001)	0.9413 (0.001)	0.9257 (0.001)	0.9413 (0.001)	0.9409 (0.001)
repvgg-a2→	0.9432 (0.001)	0.9432 (0.001)	0.9413 (0.001)	0.9471 (0.001)	0.9476 (0.001)	0.9474 (0.001)
repvgg-a2	0.9482 (0.001)	0.9482 (0.001)	0.9484 (0.001)	0.9469 (0.001)	0.9476 (0.001)	0.9471 (0.001)
resnet20→	0.9482 (0.001)	0.9482 (0.001)	0.9484 (0.001)	0.9279 (0.001)	0.9458 (0.001)	0.9458 (0.001)
resnet56→	0.9482 (0.001)	0.9482 (0.001)	0.9484 (0.001)	0.9436 (0.001)	0.9500 (0.001)	0.9499 (0.001)

Table 11: Results for CIFAR-100 ($n_{cal} = 5000$, 10 trials). The best result(s) for each model (within 1 standard error) are in bold. → indicates the use of a different representation to calibrate the previous model.

Brier score						
Model	Uncal.	TS	Hist bin	SBA	SWC	SWC-HH
resnet20	0.4527 (0.002)	0.4328 (0.001)	0.4929 (0.002)	0.5352 (0.001)	0.4684 (0.002)	0.4677 (0.002)
resnet56→	0.4527 (0.002)	0.4328 (0.001)	0.4929 (0.002)	0.4313 (0.001)	0.4404 (0.002)	0.4400 (0.002)
repvgg-a2→	0.4527 (0.002)	0.4328 (0.001)	0.4929 (0.002)	0.3431 (0.001)	0.3281 (0.001)	0.3280 (0.001)
resnet56	0.4210 (0.002)	0.3862 (0.001)	0.4466 (0.002)	0.4335 (0.002)	0.4192 (0.002)	0.4184 (0.002)
resnet20→	0.4210 (0.002)	0.3862 (0.001)	0.4466 (0.002)	0.5239 (0.001)	0.4156 (0.002)	0.4133 (0.003)
repvgg-a2→	0.4210 (0.002)	0.3862 (0.001)	0.4466 (0.002)	0.3431 (0.001)	0.3222 (0.001)	0.3221 (0.001)
repvgg-a2	0.3267 (0.001)	0.3257 (0.001)	0.3783 (0.001)	0.3433 (0.001)	0.3326 (0.001)	0.3313 (0.001)
resnet20→	0.3267 (0.001)	0.3257 (0.001)	0.3783 (0.001)	0.5213 (0.001)	0.3467 (0.001)	0.3451 (0.001)
resnet56→	0.3267 (0.001)	0.3257 (0.001)	0.3783 (0.001)	0.4245 (0.001)	0.3417 (0.001)	0.3407 (0.001)
Accuracy						
Model	Uncal.	TS	Hist bin	SBA	SWC	SWC-HH
resnet20	0.6809 (0.001)	0.6809 (0.001)	0.6752 (0.002)	0.6098 (0.001)	0.6738 (0.001)	0.6738 (0.001)
resnet56→	0.6809 (0.001)	0.6809 (0.001)	0.6752 (0.002)	0.6914 (0.001)	0.6912 (0.001)	0.6912 (0.001)
repvgg-a2→	0.6809 (0.001)	0.6809 (0.001)	0.6752 (0.002)	0.7592 (0.001)	0.7663 (0.001)	0.7662 (0.001)
resnet56	0.7225 (0.001)	0.7225 (0.001)	0.7176 (0.001)	0.6911 (0.001)	0.7171 (0.001)	0.7169 (0.001)
resnet20→	0.7225 (0.001)	0.7225 (0.001)	0.7176 (0.001)	0.6209 (0.002)	0.7200 (0.001)	0.7197 (0.001)
repvgg-a2→	0.7225 (0.001)	0.7225 (0.001)	0.7176 (0.001)	0.7594 (0.001)	0.7710 (0.001)	0.7710 (0.001)
repvgg-a2	0.7725 (0.001)	0.7725 (0.001)	0.7622 (0.001)	0.7591 (0.001)	0.7651 (0.001)	0.7651 (0.001)
resnet20→	0.7725 (0.001)	0.7725 (0.001)	0.7622 (0.001)	0.6222 (0.001)	0.7668 (0.001)	0.7666 (0.001)
resnet56→	0.7725 (0.001)	0.7725 (0.001)	0.7622 (0.001)	0.6961 (0.001)	0.7688 (0.001)	0.7686 (0.001)